



# OPEN Impact of built environment on commuting carbon emissions using big data: a case study of Jinan's main urban area

Yukang Li<sup>1</sup>, Jianming Ye<sup>1,2</sup>✉, Zhaoqi Li<sup>1</sup>, Mengmeng Zhu<sup>1</sup> & Yingbin Li<sup>1,3</sup>

Rapid urbanization and alterations in the built environment have exacerbated transportation energy consumption and environmental pollution, making transportation-related carbon emissions a significant barrier to low-carbon urban development. This study examines the influence of the built environment on commuting carbon emissions in the central urban area of Jinan, addressing the increasing challenge of transportation-induced emissions in rapidly urbanizing cities. Through the integration of multi-source big data, including travel trajectory, urban land use, and street view data, the research analyzes the spatial patterns of commuting behavior and emissions. Utilizing spatial autocorrelation, multiple linear regression, and geographically weighted regression (GWR), the study identifies critical factors influencing emissions, such as residential and commercial land area, transportation hubs, road network density, and floor area ratio. The results reveal that commuting emissions exhibit a monocentric pattern, with higher emissions in suburban areas due to lower population density and limited access to public transportation. Conversely, the central urban area of Jinan experience lower emissions, attributed to greater use of public transportation and shorter commuting distances. The GWR model uncovers spatial heterogeneity in the impact of the built environment, emphasizing the necessity for context-specific urban planning strategies. This research presents a comprehensive framework for reducing commuting carbon emissions, providing valuable insights for medium-sized cities striving to promote low-carbon transportation and optimize urban structures. The findings contribute to the formulation of targeted, data-driven policies for sustainable urban planning.

**Keywords** Commuting carbon emissions, Built environment, Geographical weighted regression, Geographic detector

China has set the goal of reaching peak carbon emissions by 2030 and achieving carbon neutrality by 2060. However, carbon emissions from the transportation sector account for 10% of the national total and are increasing rapidly, making them the third-largest source of greenhouse gas emissions<sup>1,2</sup>. Compared to the industrial and building sector, the progress in reaching the carbon peak in transportation lags behind, and the challenges of reducing emissions are more pronounced<sup>3</sup>. High-frequency, regular commuting behavior exacerbates congestion and carbon emissions, making it a critical area for breakthroughs in low-carbon transformation<sup>4</sup>. The built environment, through its spatial structure, land use layout, and transportation infrastructure, influences residents' travel modes, distances, and frequency, becoming a key factor driving transportation carbon emissions<sup>5</sup>. In commuting research, big data can be employed to reveal commuting characteristics such as travel modes and distances<sup>6</sup>, reflecting commuting flows across cities, streets, communities, and grids<sup>7</sup>. Thus, analyzing the relationship between commuting carbon emissions and the built environment using multi-source big data is a crucial scientific approach for uncovering the driving factors of commuting emissions and facilitating precise emission reductions.

Early research on commuting carbon emissions was grounded in New Urbanism theory, which highlights population density, mixed land use, and pedestrian-friendly design as strategies to reduce dependence on motor vehicles<sup>8,9</sup>. The "5D" dimensions have been widely employed to quantify the influence of the built environment

<sup>1</sup>Agricultural College, Shihezi University, Shihezi 832000, China. <sup>2</sup>College of Architecture and Urban Planning, Tongji University, Shanghai 200092, China. <sup>3</sup>College of Horticulture and Forestry Sciences, Huazhong Agricultural University, Wuhan 430070, China. ✉email: 2110309@tongji.edu.cn

on travel patterns. Existing studies have primarily focused on macro-scale indicators such as population density and road networks<sup>10,11</sup>, with limited attention given to the potential effects of the street-level microenvironment on travel behavior and route choices. Research has largely relied on statistical yearbooks or survey data<sup>12</sup>, although mobile signaling and GPS trajectory data are increasingly being utilized<sup>13</sup>. However, integrating multi-source data still faces challenges related to standardization and data interoperability<sup>14</sup>. Existing models predominantly rely on linear regression or structural equation modeling, assuming spatial homogeneity in the built environment's impact on carbon emissions, while overlooking the moderating role of local geographic contexts<sup>15,16</sup>.

Big data technology offers high-resolution analytical tools for urban studies<sup>17</sup>. Navigation data can accurately extract commuting origin–destination (OD) pairs and route choice preferences<sup>18</sup>, while street view images, analyzed through deep learning, can automatically extract street-level physical characteristics<sup>19</sup>. However, scholars have found that data such as street view images, points of interest (POI), and housing prices exhibit heterogeneity, and existing research often relies on single data sources in isolation, lacking cross-modal correlation analysis<sup>20</sup>. Ensemble learning models, such as XGBoost, are widely used to improve prediction accuracy, but their “black-box” nature can lead to feature importance rankings influenced by multicollinearity or overfitting<sup>21</sup>. Some researchers have sought to enhance interpretability through SHAP values, but their application in commuting carbon emissions research remains limited<sup>22</sup>.

Existing case studies primarily focus on megacities such as Beijing and Chengdu, and the applicability of their conclusions to medium-sized cities remains questionable<sup>23</sup>. Medium-sized cities are in a transitional phase from “single-center expansion” to “multi-center clusters<sup>24</sup>”, with suburbanization and residence-work separation coexisting<sup>25</sup>. These cities often implement a “spatial structure optimization-transportation system upgrading” collaborative strategy to avoid high-carbon lock-in effects<sup>26</sup>. However, there is currently a lack of detailed carbon emission driver maps for these cities, leading to a “one-size-fits-all” approach in policy design<sup>27</sup>.

The current research faces several limitations regarding data sources, particularly the lack of a comprehensive and multi-dimensional built environment indicator system. Additionally, there are technical challenges exist in data integration and spatial modeling, and empirical studies on low-carbon pathways in medium-sized cities remain limited. Therefore, the focus of this study is as follows: (1) Using multi-source data, such as commuting trajectory big data and semantic segmentation street view images, this research seeks to address the limitations of one-sidedness associated with traditional single-source data. (2) In response to the limitations of existing built environment indicators, the study incorporates socio-economic factors, street view perceptions, and urban land use conditions, providing a more detailed depiction of multi-dimensional built environment indicators. (3) Through stepwise variable selection, the study identifies key indicators influencing commuting carbon emissions at residential and workplace areas, and analyzes the spatial heterogeneity of these factors using geographically weighted regression models. (4) Using geographic detectors and the XGBoost framework, the study explores the interaction effects and importance rankings of these indicators, aiming to offer tailored policies and recommendations for low-carbon development in medium-sized cities.

## Data and methods

### Research framework

The study begins by extracting commuting characteristics such as commuting modes, commuting time, and commuting distance from Baidu commuting trajectory data. It then calculates the total and per capita commuting carbon emissions at street level. By extracting multiple data indicators, a built environment research framework is established. The study proceeds by summarizing the spatial correlation patterns of commuting data and the spatial distribution of commuting carbon emissions, applying spatial autocorrelation analysis methods to explore the spatial clustering features of commuting carbon emission indicators. Stepwise linear regression is used to select built environment variables, and a geographically weighted regression model is developed to analyze the spatial differential impacts of the built environment. Finally, geographic detectors are applied to investigate the interaction effects of the selected variables on commuting carbon emissions, and XGBoost is used to visualize the importance rankings of influencing factors, providing quantitative evidence for policy formulation (Fig. 1).

The fishnet approach discretizes continuous space into regular grids, eliminating spatial statistical biases caused by irregular administrative boundaries and accurately capturing spatial differentiation<sup>28</sup>. Floor area ratio, defined as the ratio of total building area to land area, reflects the intensity of land development. Geometric calculations ensure precision, avoiding indirect estimation errors<sup>29</sup>. Dijkstra's algorithm iteratively expands from the origin to the nearest unvisited node, utilizing a priority queue to ensure the optimal path, making it suitable for simulating commuting route choices<sup>30</sup>. XPath, through path expressions, precisely locates target nodes in HTML/XML documents, providing a structured, automated solution for extracting housing price information<sup>31</sup>. Gong Peng et al.<sup>32</sup> broke through the limitations of single remote sensing classification by leveraging data complementarity, providing reliable basic data for urban land use in construction areas. The fishnet analysis, computational geometry, Dijkstra's algorithm, and other methods are general paradigms in spatial analysis, requiring only the replacement of basic data to reproduce results. XPath parsing logic adapts to different website structures, and ResNet50 can be replaced with other CNN architectures to accommodate computational resource constraints.

### Research area and data

#### Research area

Jinan, the capital of Shandong Province and a key city in the Yellow River Basin, leverages its position as a transportation hub within the “Beijing-Shanghai Corridor” to shape its commuting patterns, which are characterized by “high mobility and multi-center work-residence separation<sup>33</sup>”. As of August 2024, the city's total number of private vehicles has reached 4.04 million, including approximately 3.47 million cars and 223,000 new

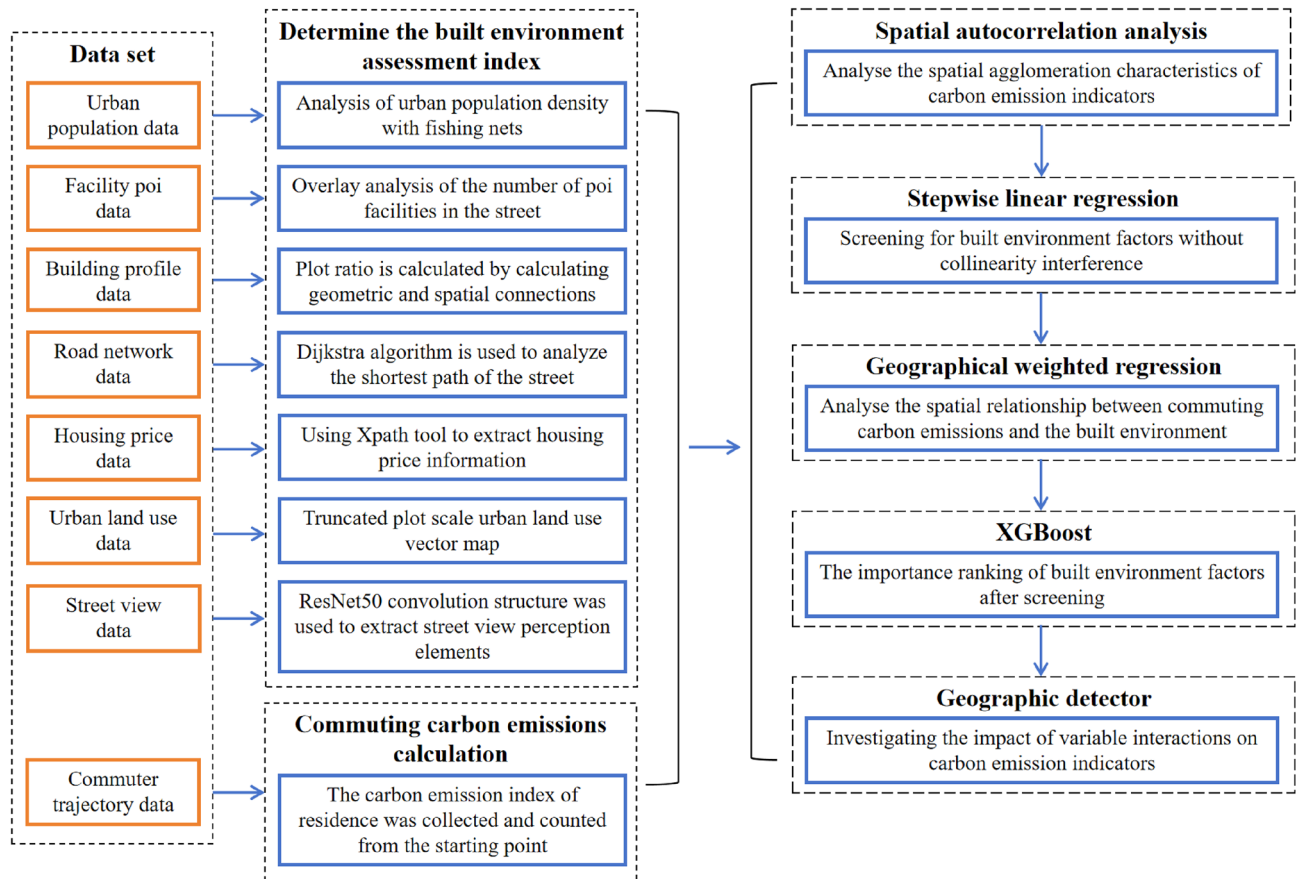


**Fig. 1.** Research framework.

energy vehicles. The commuting structure reflects a complex coexistence of “high-carbon” and “low-carbon” components<sup>34,35</sup>. The city’s transportation network is based on a “three-ring, twelve-radial” high-speed road framework, with peak congestion on the main roads exceeding 90%, and a distinct tidal commuting pattern. The density of the rail transit network is relatively low compared to cities of similar size, and bus coverage in peripheral areas remains insufficient<sup>36–38</sup>.

This study focuses on the central urban area of Jinan City (Jinan Urban Master Plan 2016–2035). The total area is approximately 720 square kilometers, with a population of 4.35 million (Fig. 2). The map is based on the standard map (Lu SG(2023)026) downloaded from the Standard Map Service website of the Ministry of Natural Resources of China, without modifications to the base map.

#### Data

**Commuter trajectory data** In this study, users’ commuting patterns were mined based on long-term time-series user behavior data, and path planning algorithms were used to restore possible commuting paths in the context of known places of employment, residence and commuting patterns. Combining the static origin and destination (OD) and trajectory recovery data, the travel segment is identified by spatial density clustering and other methods, the travel chain is extracted, and the commuter distribution and commuter behavior characteristics are obtained by analyzing the segmented travel characteristics. The specific methodological framework is shown in Fig. 3. The study recovered 3.52 million commuting trajectories for 4.92 million people in November 2024. Attributes such as OD trajectory point coordinates, travel time and travel mode contained in the commuting trajectory data can effectively support the calculation of subsequent commuting carbon emissions<sup>39</sup>. Appendix Fig. 1 and Appendix Fig. 2 illustrate commuting modes and commuting time data within the study area.

**Street view perception data** To obtain the required data, the Baidu Maps API (<https://map.baidu.com/>) was used to capture street view images along the road network of Jinan City. The selected points were distributed across different regions of the city, as illustrated in Fig. 4. At each point, four street view images were collected from different angles; however, a small number of locations lacked 360-degree image coverage. In total, 154,020 street view images were collected for the extraction of streetscape elements.

Figure 5 presents the convolutional architecture of ResNet50, which processes input images through multiple stages of downsampling to generate feature maps at different scales. These feature maps are subsequently integrated to construct a comprehensive representation for segmentation<sup>40,41</sup>. The downsampling operation in ResNet50 is implemented using convolutional layers with a stride of 2 and 3×3 kernel size, ensuring the

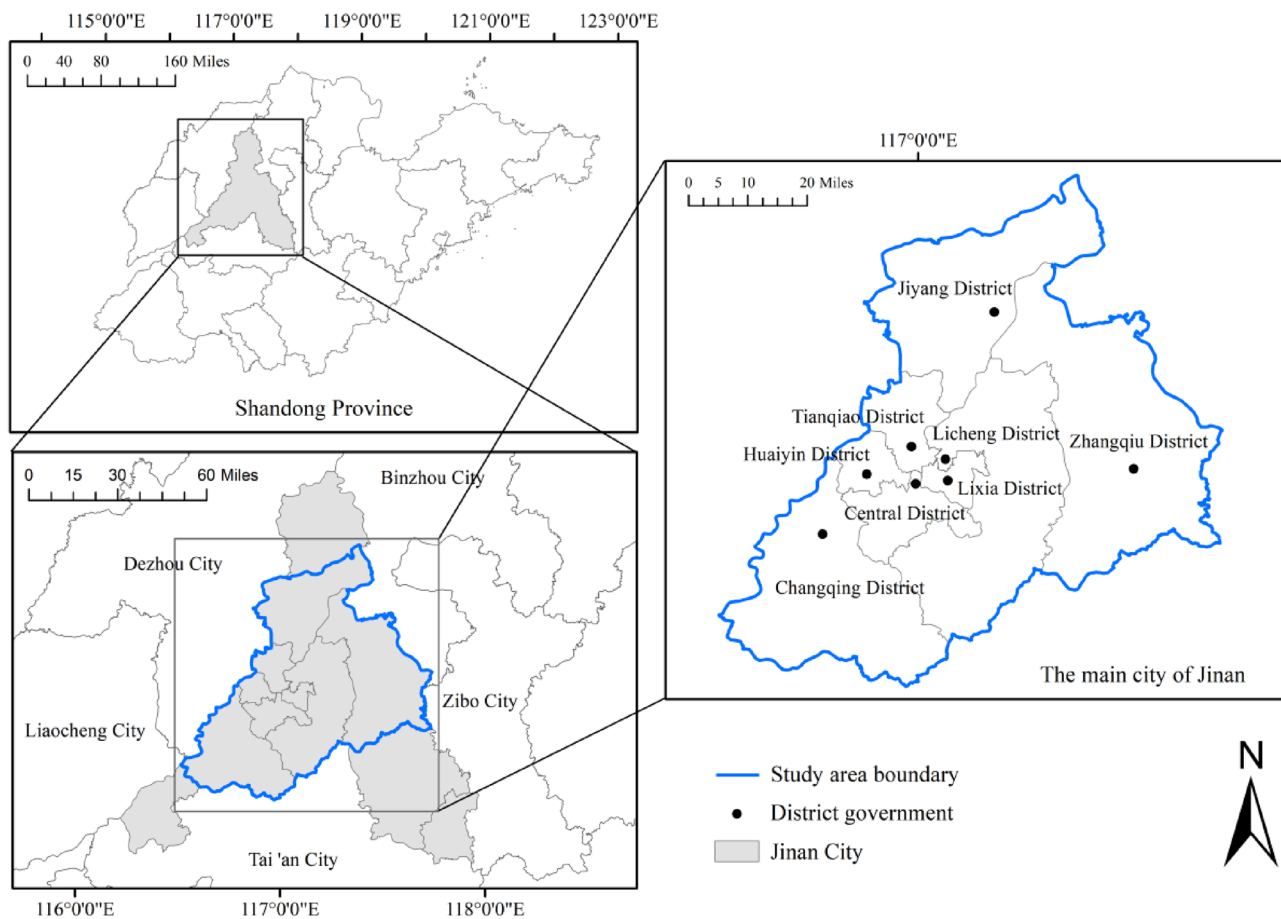


**Fig. 2.** Study area.

alignment of scales across different feature maps. Bilinear interpolation is employed for both the downscaling and upscaling of feature map dimensions, followed by a  $1 \times 1$  convolutional layer to fuse the final feature map. The ResNet50 architecture effectively combines feature maps from various scales at each stage of scale transition, thereby preserving and enhancing multiscale image features, ultimately optimizing the retention of detailed information across multiple resolutions<sup>42</sup>.

Drawing on references<sup>43,44</sup>, nine street-view element indicators were chosen to depict the built environment (Fig. 6). These indicators can be classified into two types: objective visual perceptions and subjective emotional perceptions. The three visual indicators of openness, greenness and traffic signs are calculated directly from the components of different features. Table 1 presents the calculation formulas and concise descriptions of these visual perception indicators. The other six indicators represent emotional perceptions, such as beauty, boredom, depression, safety, liveliness, and wealth. These are obtained by establishing a rating model based on machine-learning algorithms. The features employed to train this model are also extracted from various ground-object components<sup>45</sup>. For the development of the rating model, an emotional-perception dataset from<sup>46</sup> was employed (Fig. 7).

**Built environment data** This study referred to the “5D” dimension of the built environment<sup>47</sup>, and added socio-economic attributes<sup>48</sup>, urban land use level<sup>49</sup> and streetscape elements into the data set.

The built environment data set was constructed from seven aspects: density, points of interest richness, design, destination proximity, socioeconomic attributes, urban land use and street view perception. For details, see Table 2. Appendix Fig. 3 illustrates the built environment data within the study area.

The multi-source data used in this study include population data, facility point of interest (POI) data, urban road network data, building profile data, urban housing price data, and urban land use data of Jinan City, as detailed in Table 3.

Gong Peng et al.<sup>32</sup> conducted China’s land use mapping by comprehensively utilizing remote sensing data, night light data, Internet location data, and point of interest data. In this study, the original data are simplified into five categories of first-level land classification, including residential, commercial, industrial, public service facilities, and transportation land (Fig. 8). The Maximum Patch Proportion, Spread Degree, Shannon Diversity, and Degree of Agglomeration were employed to calculate the land use characteristics in the study area. As presented in Table 3, the maximum patch proportion represents the percentage of the largest single patch in the total area of the study area. The spread degree indicates the spatial diffusion or aggregation of land use patch

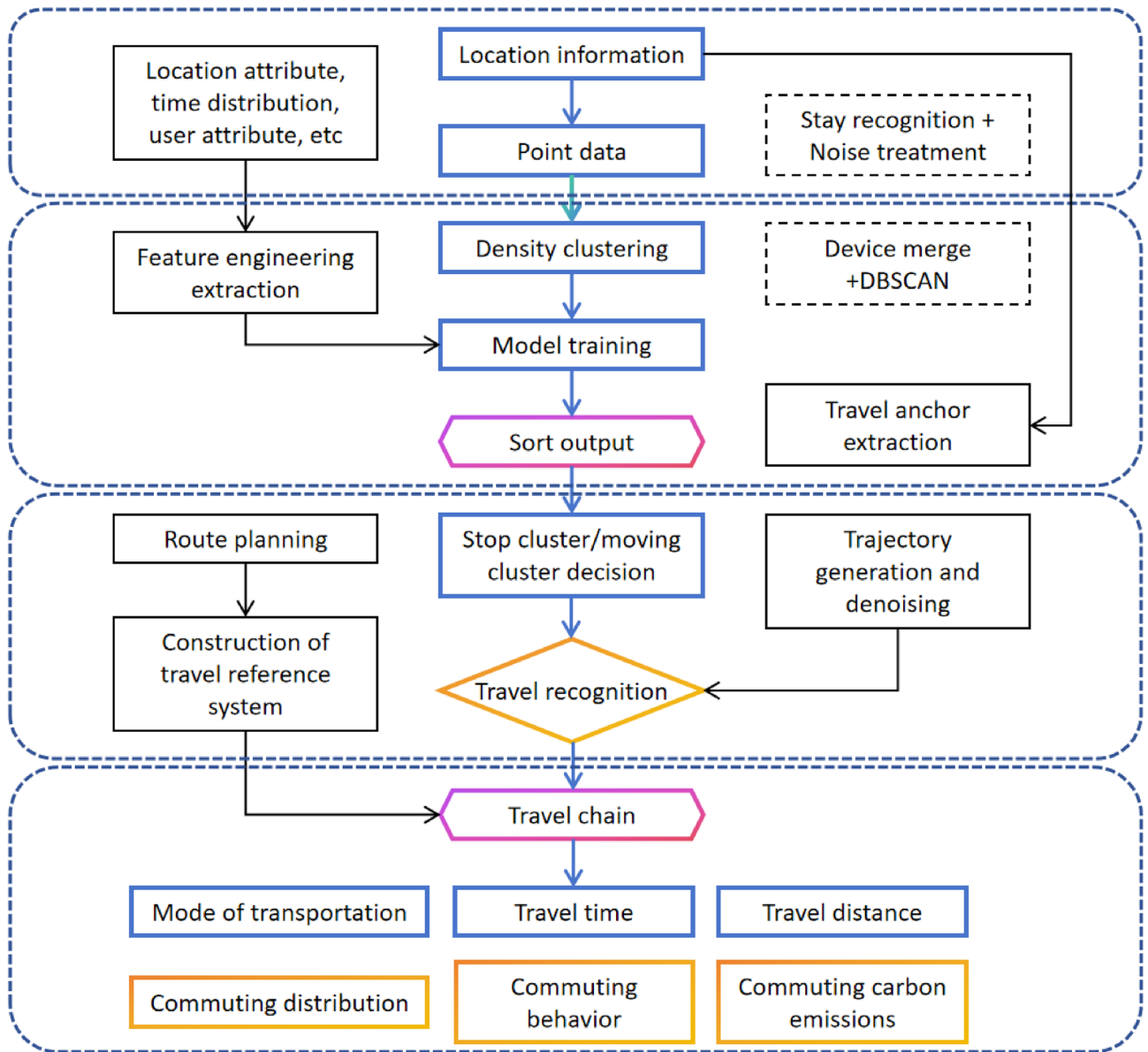


Fig. 3. Commuter trajectory extraction diagram.

types, while Shannon diversity measures the diversity and evenness of patch types. The degree of clustering quantifies the spatial clustering of similar patch types.

### Research methods

#### Calculation method of commuting carbon emission

To accurately estimate commuting carbon emissions in the main urban area of Jinan, this study employs a “bottom-up” approach. By multiplying the carbon emission factors of each commuting mode by the corresponding commuting distance, individual daily commuting carbon emissions are calculated. Based on commuting trajectory OD data, the total commuting carbon emissions at the street level are calculated using residential locations (O) and workplaces (D) as spatial units. This approach provides a clearer understanding of the differential impacts of the built environment at residential and workplace locations on commuting carbon emissions, facilitating the precise identification of emission sources<sup>50</sup>. Commuter travel emissions are calculated based on commuting mode and distance, as expressed in the specific formula provided in Eq. (1). The calculation for daily commuter carbon emissions is as follows:

$$T_n = \sum_{i=1}^n D_i \times K_i \tag{1}$$

where:  $T_n$  is the total carbon emission of a commuter in a single day (g);  $i$  is a certain mode of transportation;  $D_i$  is the total distance (km) traveled by the mode of transportation  $i$ ;  $K_i$  is the (g/ person · km). The transportation

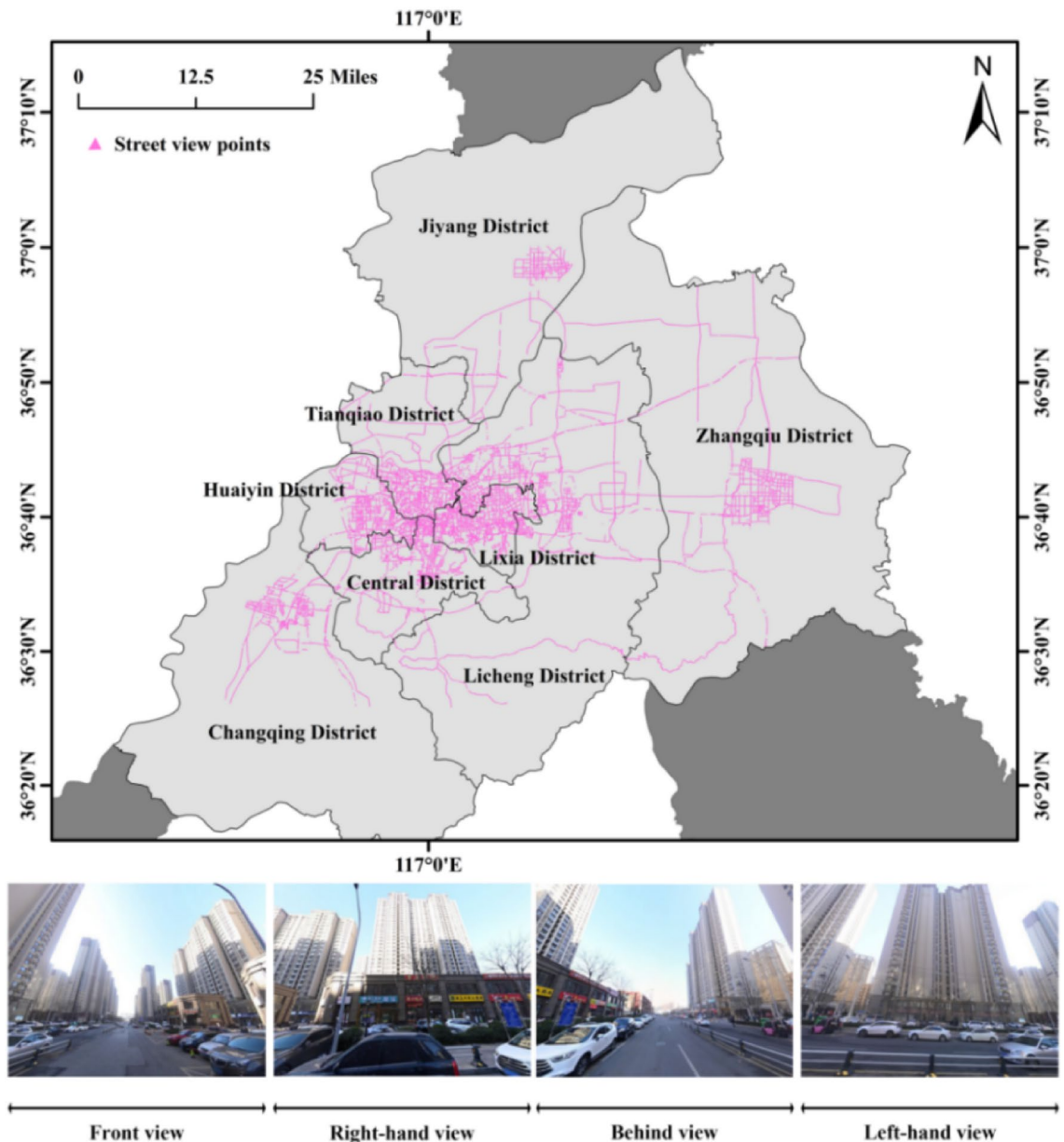


**Fig. 4.** Spatial distribution of shooting points for requesting street view images.

modes in this study are divided into three categories: driving, public transportation and green commuting. The traffic travel distance is calculated by track OD points and path data in path planning.

In this study, the carbon emission factor values of different transportation modes were determined according to the Set of Greenhouse Gas Emission Coefficients of Chinese Products throughout their life Cycle (2022) released by the Ministry of Ecology and Environment in 2022, and the relevant data of Shandong Province were verified. The carbon emission factors of different commuting modes used in this study are shown in Table 4.

In parallel, considering the rapid adoption of new energy vehicles, the study obtained ownership data for both traditional fuel vehicles and new energy vehicles by referring to the Statistical Bulletin of National Economic and Social Development of Jinan City. The study further estimated the level of carbon emissions generated by private cars during commuting by incorporating the proportion of vehicle types.

As of November 2024, Jinan has opened and operated three subway lines, covering a total distance of approximately 96.335 km with 46 stations. Given the relatively small number of subway lines and the short operation period of the subway system, fluctuations in subway operational efficiency has not had a significant impact on the overall transportation system. As the study aims to analyze the characteristics of residents' commuting carbon emissions, factors such as ride-sharing car commuting, temporal variations in traffic carbon emissions, vehicle type differences, and indirect carbon emissions are not considered in the calculation process.

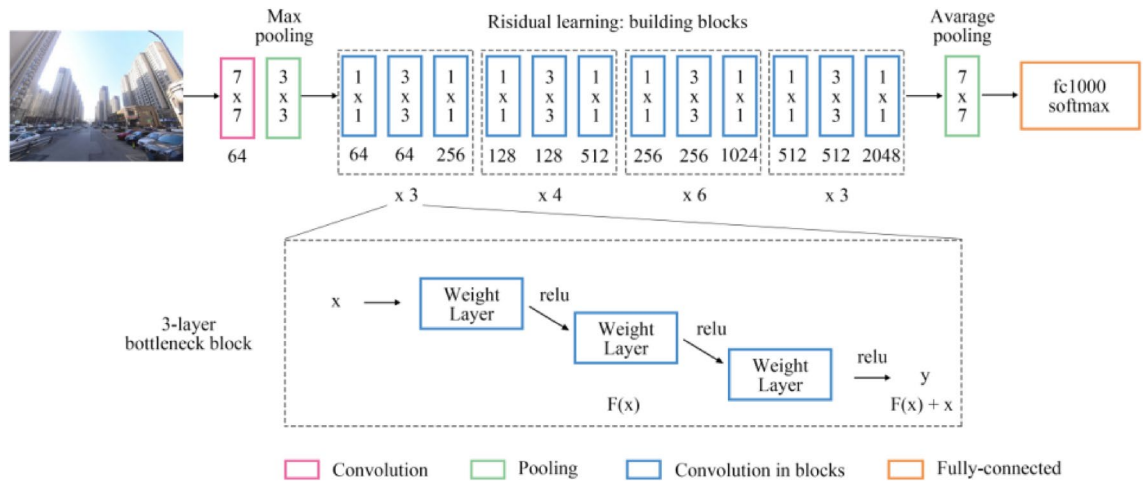


Fig. 5. Simplified ResNet50 architecture with a depiction of building blocks.

*Spearman correlation test*

To verify the accuracy of commuter carbon emissions calculated using the top-down method, 395,400 signaling data points provided by mobile phone operators (MPSD) in November 2024 were used as an additional data source to capture travel patterns in the main urban area of Jinan City. Spearman correlation analysis was employed to assess the relationship between the top-down estimates values and those derived from signaling data. Spearman correlation analysis is widely used to measure the monotonic association between variables, with a higher correlation coefficient indicating a stronger correlation<sup>51</sup>. It is also suitable for analyzing variables that are not normally distributed. As shown in Table 5, the correlation coefficients of commuting data obtained from different data sources within the same category exceeds 0.8, demonstrating the effectiveness of the commuting carbon emissions calculation method.

*Spatial autocorrelation analysis*

In this study, ArcGIS was used to correlate OD points with street attributes to calculate the street-scale commuting carbon emission index. GeoDa 1.18 was used to analyze the Moran index and hotspots of commuter carbon emissions and travel modes in the main urban area of Jinan City, obtaining the spatial distribution characteristics of commuter carbon emissions and travel modes<sup>52</sup>. The calculation formula is as follows<sup>53</sup>:

$$Moran's\ I = \frac{\sum_{i=1}^n \sum_{j=1}^n W_{ij} (X_i - \bar{X}) (X_j - \bar{X})}{S^2 \sum_{i=1}^n \sum_{j=1}^n W_{ij}} \tag{2}$$

$$Gi^* = \frac{\sum_{j=1}^N W_{ij} \cdot X_j - \bar{X} \sum_{j=1}^N W_{ij}}{\sqrt{\frac{\sum_{j=1}^N X_j^2}{N} - (\bar{X})^2} \cdot \sqrt{\frac{N \sum_{j=1}^N W_{ij}^2 - \left(\sum_{j=1}^N W_{ij}\right)^2}{N-1}}}, \forall j \neq i \tag{3}$$

In the Eqs. (2) and (3), N is the number of streets.  $X_i, X_j$  are the carbon emissions of the street.  $\bar{X}$  is the average carbon emission of X, and  $W_{ij}$  represents the spatial weight matrix between street i and street j.

The value range of Moran's I is [-1, 1]. Moran's I > 0 indicates spatial positive correlation, where the research objects exhibit spatial clustering. When Moran's I < 0, it indicates spatial negative correlation, and the object of study is spatially discrete. When Moran's I = 0, the study objects are randomly distributed.

*Stepwise linear regression*

In order to further analyze the relationship between urban built environment factors and commuting carbon emissions, this study adopted the stepwise regression method to screen indicators, and established a linear regression model using the screened indicators. The calculation formula is as follows<sup>54</sup>:

$$Y = \beta_0 + \beta_1 x_1 + \beta_2 x_2 + \dots + \beta_i x_i + \varepsilon \tag{4}$$

$\beta_0$  is a constant coefficient;  $\beta_{(1,2,\dots,i)}$  is the independent variable coefficient;  $\varepsilon$  is the residual; Suppose that  $H_0: \beta_{(1,2,\dots,i)} = 0$ , and the collected samples are used to test the significance of F statistic (or t statistic) for  $H_0$ .

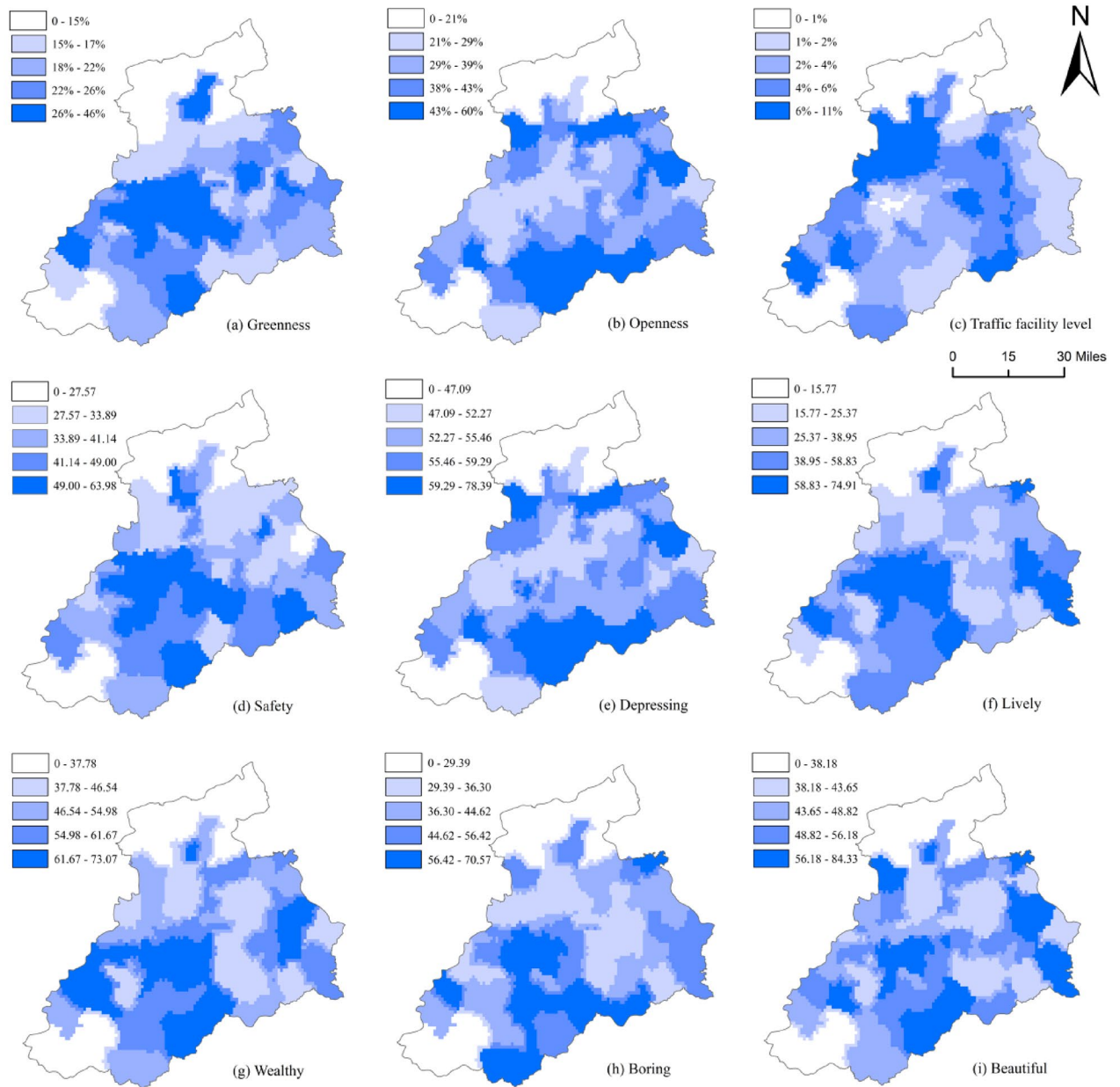


**Fig. 6.** Streetscape elements distribution.

Indicators	Formula	Introduction
Openness	$Openness = P_s$	Openness is defined as the proportional contribution of sky elements within the scene, whereas Pixel Sky ( $P_s$ ) quantifies the percentage of sky pixels in image data
Greenness	$Greenness = P_v$	Greenness is defined as the vegetation coverage within the visual field, serving as a metric to quantify the urban street greening level through land cover composition analysis. $P_v$ represents the proportion of vegetation pixels
Traffic sign	$Traffic\ sign = P_{TS}$	Traffic signs refer to the facilities used to manage traffic, ensure road safety and assist vehicles to pass smoothly. $P_{TS}$ represents the proportion of traffic sign pixels

**Table 1.** Formulas and introductions for visual perceptions.

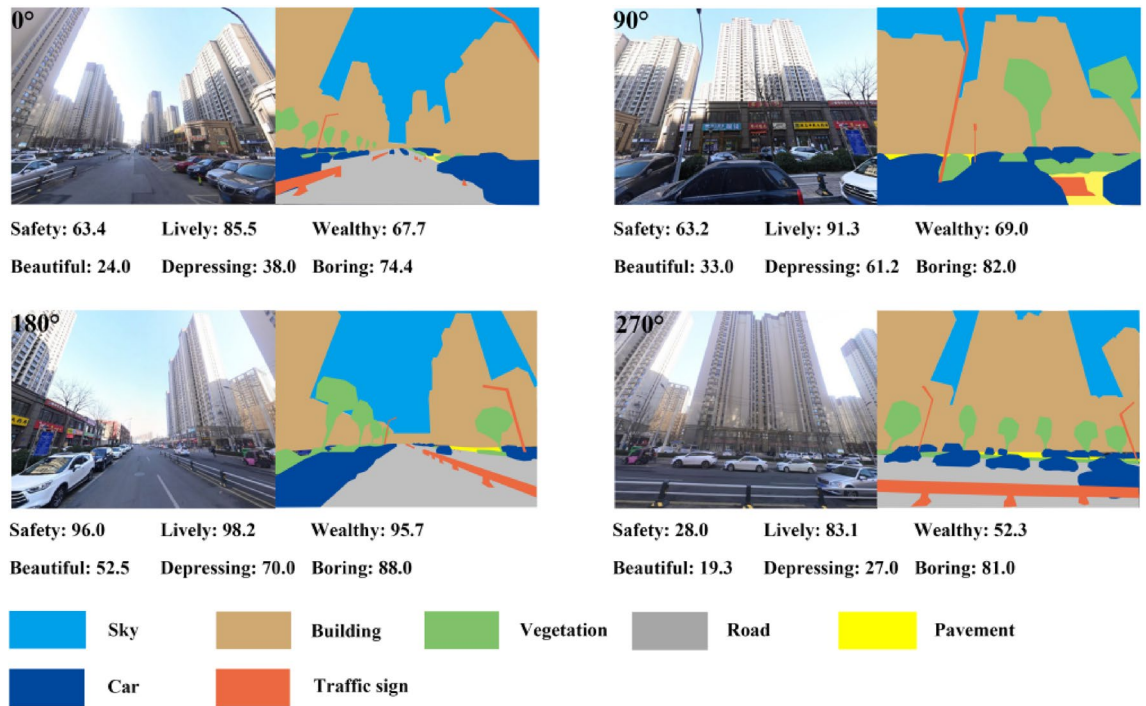


Fig. 7. Examples of semantic segmentation.

$$F = \frac{\sum_{i=1}^n (\hat{y}_i - \bar{y})^2 / m}{\sum_{i=1}^n (\hat{y}_i - \bar{y})^2 / (n - m - 1)} \tag{5}$$

For a given confidence  $\alpha$  (usually 95%), the statistic F should be:

$$p(F \leq F_{\alpha}(m, n - m - 1)) \leq 1 - \alpha \tag{6}$$

If formula (6) is not valid, then the hypothesis is considered to be invalid and the regression equation is considered significant.

*Geographically weighted regression*

This study used geographically weighted regression (GWR) to reveal the spatial non-stationarity and spatial heterogeneity of influencing factors for commuter carbon emissions<sup>55</sup>. The model was as follows:

$$y_i = \beta_0(u_i, v_i) + \sum_{i=1}^k \beta_i(u_i, v_i) x_{ik} + \varepsilon_i \tag{7}$$

where:  $y_i$  is the dependent variable,  $(u_i, v_i)$  is the geographic coordinates of the  $i$ -th sample space unit, the parameter  $\beta_i$  varies with location,  $x_{ik}$  is the independent variable, and  $\varepsilon_i$  is the random error term. In this study, the Gaussian function method was selected and Akaike information criterion (AICc) was used as the selection criterion for the model. Model diagnostic tests is used to evaluate the prediction accuracy and stability of the model, and its calculation formula is as follows:

$$\omega_{ij} = \exp \left[ -\left( d_{ij} / b \right)^2 \right] \tag{8}$$

where,  $\omega_{ij}$  is the weight of the variable of sample space unit  $j$  relative to street  $i$ ,  $d_i$  is the distance between two points, and bandwidth  $b$  is a non-negative attenuation parameter describing the functional relationship between weight and distance.

*Geographic detector model*

The geographic detector model (GDM) provides a convenient way to examine the mechanisms of commuting carbon emissions. The basic idea of GDM is that when one or more variables have a significant impact on commuting carbon emissions, the independent variables should have a spatial pattern similar to that of commuting carbon emissions. The advantage of GDM is that it can assess the interactive effects of two factors on commuting carbon emissions<sup>56</sup>. The calculation formula is as follows:

Dimension	Variable	Unit	Description
Density	Population density (PD)	people /km <sup>2</sup>	Refers to the number of people per unit area, used to reflect the degree of population concentration
Various interest points enrichment level	Food and beverage items (FBI)		Refers to the number of various points of interest in the street, indicating the richness of the facilities
	Exercises (EX)		
	Medical care (MC)		
	Recreation (RE)		
	Companies (CO)		
	Shopping consumption (SS)		
	Financial institutions (FI)		
	Hotel accommodations (HA)		
	Science, education and culture (SEC)		
	Tourist attractions (TA)		
	Life services (LS)		
Commercial residences (CR)			
Design	Plot ratio (PR)		Refers to the ratio of the total construction area of a space unit to its land area, used to indicate the intensity of land use and development
	Road density (RD)	km/km <sup>2</sup>	Refers to the length of urban roads per unit area, indicating the level of network accessibility
	Traffic congestion index (TCI)		Traffic congestion index is calculated by comparing actual travel speed with free-flow speed or time, reflecting real-time road conditions and helping to optimize travel planning and traffic governance
Destination proximity	Accessibility (AC)		Refers to the reciprocal of the average shortest time for points of interest to reach other streets, indicating the convenience of traffic locations
	Number of subway stations (NSS)		Refers to the number of transit stations along streets, indicating the accessibility of transportation
	Number of bus stops (NBS)		
	Number of other traffic stops (NOTS)		
	Density of bus stops (DBS)	per /km <sup>2</sup>	Refers to the ratio of the number of transit stations in a space unit to its land area, used to indicate the level of transportation accessibility
Density of other traffic stations (DOTS)			
Socioeconomic attribute	Average room rate (ARR)	yuan	Refers to the average housing price within a neighborhood, used to indicate the income level of the residents
	GDP	10,000 yuan/km <sup>2</sup>	Refers to the gross product of a space unit, used to indicate the economic scale and development level
Urban land use level	Land area for residential facilities (LARF)	km <sup>2</sup>	Refers to the area of various types of construction land within the urban area, indicating the composition of urban land use
	Land area for commercial facilities (LACF)		
	Land area for industrial facilities (LAIF)		
	Land area for public service facilities (LAPSF)		
	Land area for transportation facilities (LATF)		
	Residential land proportion (RLP)	%	Refers to the proportion of different types of urban land use, indicating the spatial pattern of urban land use
	Commercial land proportion (CLP)		
	Industrial land proportion (ILP)		
	Public service facilities land proportion (PSFLP)		
	Transportation facilities land proportion (TFLP)		
	Maximum patch proportion (MPP)		Refers to the landscape horizontal type landscape index of land use spatial pattern
	Spread degree (SD)		
	Shannon diversity (SD)		
	Degree of agglomeration (DA)		
Visual perceptions	Openness (OP)		Perceptual constructs of the urban environment are derived from observable physical attributes of the built environment, which serve as indicators of residential living conditions
	Greenness (GR)		
	Traffic sign (TS)		
Emotional perceptions	Beautiful (BE)		Emotional perception is a subjective rating of the living environment scored by humans, expressing residents' assessment of the quality of life
	Boring (BO)		
	Depressing (DE)		
	Safety (SA)		
	Lively (LI)		
	Wealthy (WE)		

Table 2. Built environment data.

Data name	Format	Source
Urban population	Grid	<a href="https://www.worldpop.org">https://www.worldpop.org</a>
Facility poi	Tabulation	<a href="https://lbs.amap.com">https://lbs.amap.com</a>
Road network	Vector quantity	<a href="https://www.openstreetmap.org">https://www.openstreetmap.org</a>
Building profile	Vector quantity	<a href="https://www.openstreetmap.org">https://www.openstreetmap.org</a>
Housing price	Tabulation	<a href="https://cd.lianjia.com/xiaoqu">https://cd.lianjia.com/xiaoqu</a>
Urban land use	Vector quantity	<a href="http://data.ess.tsinghua.edu.cn">http://data.ess.tsinghua.edu.cn</a>

**Table 3.** Data source.

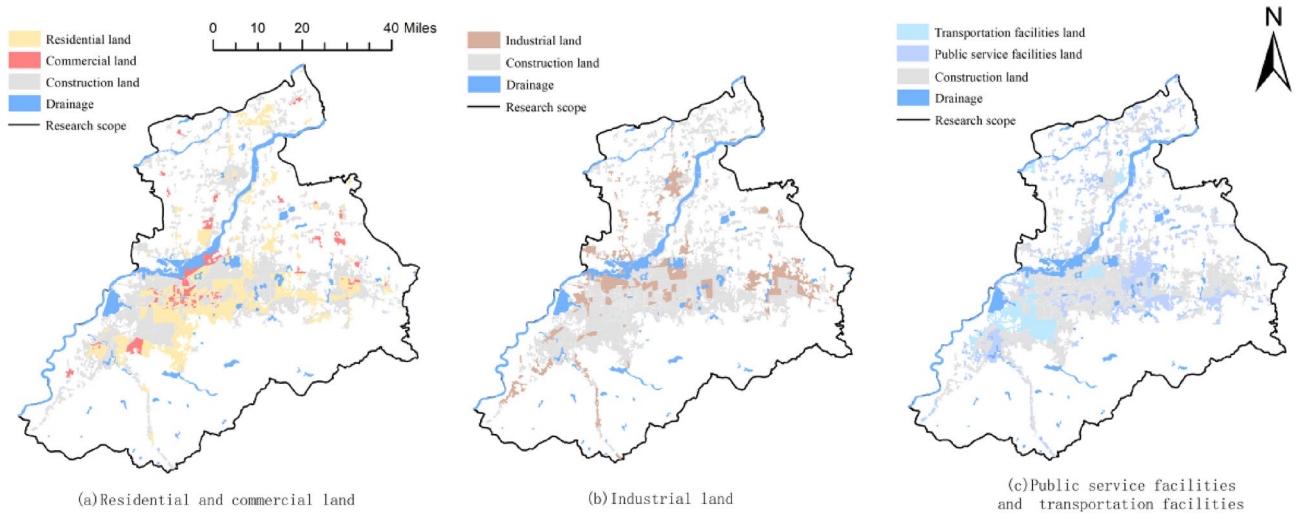


**Fig. 8.** Urban land use distribution map.

Traffic category	Mode of transportation	Carbon emission coefficient/(g/ person·km)	Carbon emission intensity
Private car commuting	Private car/Taxi	135	High
Public transport commuting	Bus/Unit shuttle/Metro	21	Middle
Green commuting	Walking/Cycling	0	Low

**Table 4.** Carbon emission factor coefficients of different traffic.

	Total residential commuting carbon emissions	Per capita commuting carbon emissions	Total carbon emissions from workplace commuting	Commuting carbon emissions per person at work
Total commuter carbon emissions (MPSD)	0.830**	0.071	0.914**	0.166
Per capita commuting carbon emissions calculated (MPSD)	-0.196*	0.883**	-0.08	0.916**
Commuting distance per capita (MPSD)	-0.373**	0.736**	-0.197*	0.811**

**Table 5.** Commuter carbon emissions testing. \*\* indicates significant at 0.01 level; \* indicates significant at 0.05 level.

$$q_{x,y} = 1 - \frac{\sum_{i=1}^m N_{X,i} \sigma_{Y_{X,i}}^2}{N \sigma_Y^2} \quad (i = 1, 2, \dots, m) \tag{9}$$

where:  $i$  represents the classification of factor  $X$ ,  $N_{X,i}$  and  $N$  denote the number of units in layer  $i$  and the total number of units in the entire area, respectively.  $\sigma_{Y_{X,i}}^2$  and  $\sigma_Y^2$  correspond to the discrete variance of  $Y$  values within layer  $i$  and across the whole region, respectively.  $q_{x,y}$  represents the explanatory power of factor  $X$  on

variable  $Y$ , where the value of  $q$  ranges from  $[0,1]$ . A value of  $q$  closer to 1 indicates a stronger explanatory power of factor  $X$  on variable  $Y$ .

#### XGBOOST algorithm

To enhance the interpretability of the selected variables, the XGBoost framework was used to analyze the importance of the influencing factors. This gradient-boosted decision tree ensemble offers improved computational efficiency and predictive performance compared to traditional gradient boosting methods<sup>57</sup>.

$$Obj = \sum_{i=1}^n L(y_i, \hat{y}_i) + \sum_{k=1}^K \Omega(f_k) \quad (10)$$

where,  $L$  is the loss function, which is used to measure the error between the predicted value  $\hat{y}_i$  and the true value  $y_i$ , and  $\Omega$  is the regularization term, which is used to control the complexity of the model and avoid overfitting.

## Results

### Analysis of commuting carbon emission characteristics

#### Analysis of commuter connection characteristics

From the spatial distribution characteristics of commuter connections (Fig. 9), the commuter flow of each street presents a single-center structure with “commuter center” as the core, and also shows a tendency to develop into a multi-center structure. As shown in the figure, the spatial visualization of commuting flow between streets with more than 500 commuters reveals the presence of multiple high-value flow areas across streets in the main urban area, which are densely distributed and have frequent commuting between workplaces and residences. The network density is high, making these areas significant employment agglomeration centers. The eastern high-tech Development Zone, the Lingang Economic Development Zone, the new materials Industry Park and other areas also maintain a high commuting links with the main city and its surrounding streets, forming a secondary employment centers.

The proportion of car commuting in the central urban area is low, such as in Beitan Street, Guanzhaying Street and Dongguan Street, while the proportion of car commuting in the peripheral areas is high, such as Daqiao Town and Cuizhai Town, and the proportion of car commuting shows a gradual increasing trend from the center to the periphery. The proportion of bus commuting is higher in the northeast than in the southwest, and the proportion of buses at the end streets of Tangye, Baiyun Lake and Huanghe Town is higher. Overall, the proportion of green commuting is higher in the southwest than in the northeast. The main reason is that the southwest is limited by the mountainous landscapes and land use patterns, resulting in lower traffic network density and bus accessibility compared to the northeast, which contributes to a higher proportion of green commuting (Fig. 10).

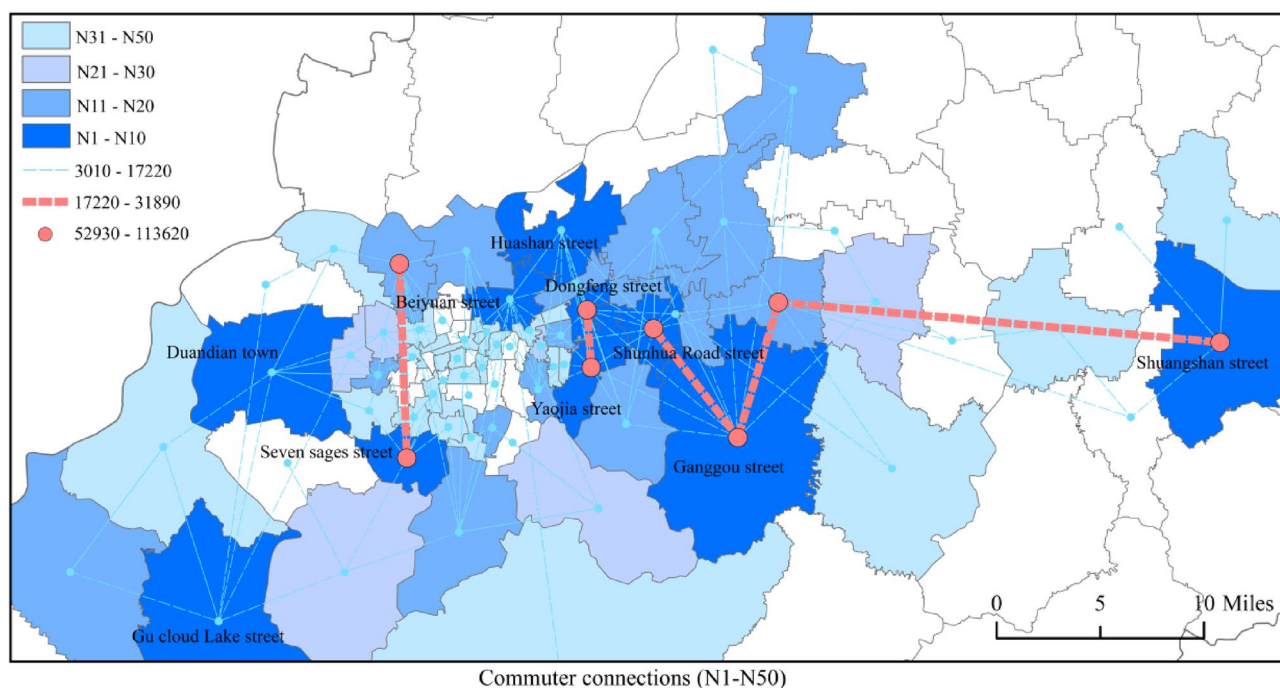


**Fig. 9.** Street to street commuter connections. The figure (N1-N50) indicates that the total number of street commutes ranks between 1 and 50. The map shows the top 10 streets for commutes.

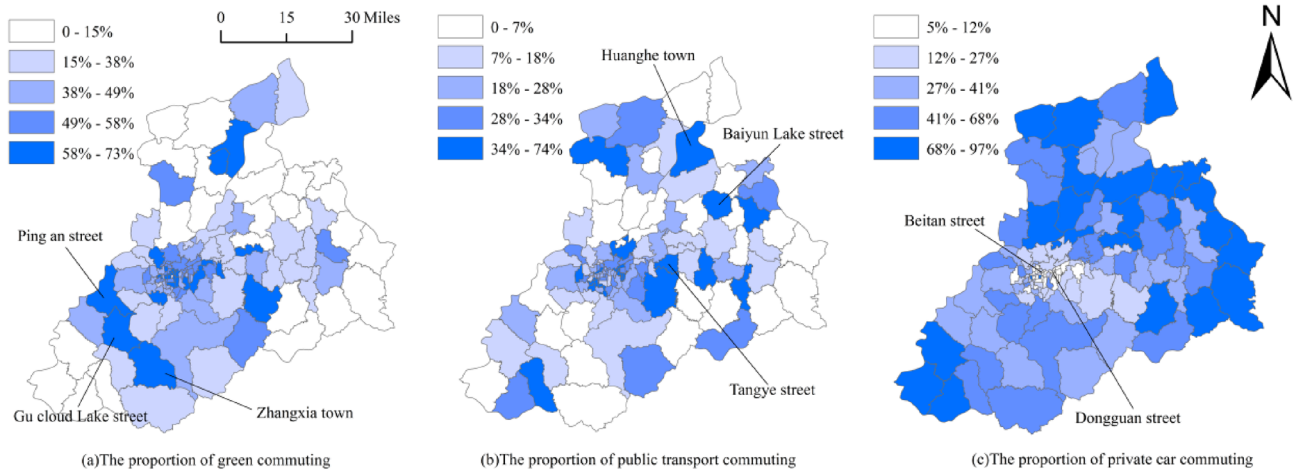


**Fig. 10.** Commuting mode distribution.

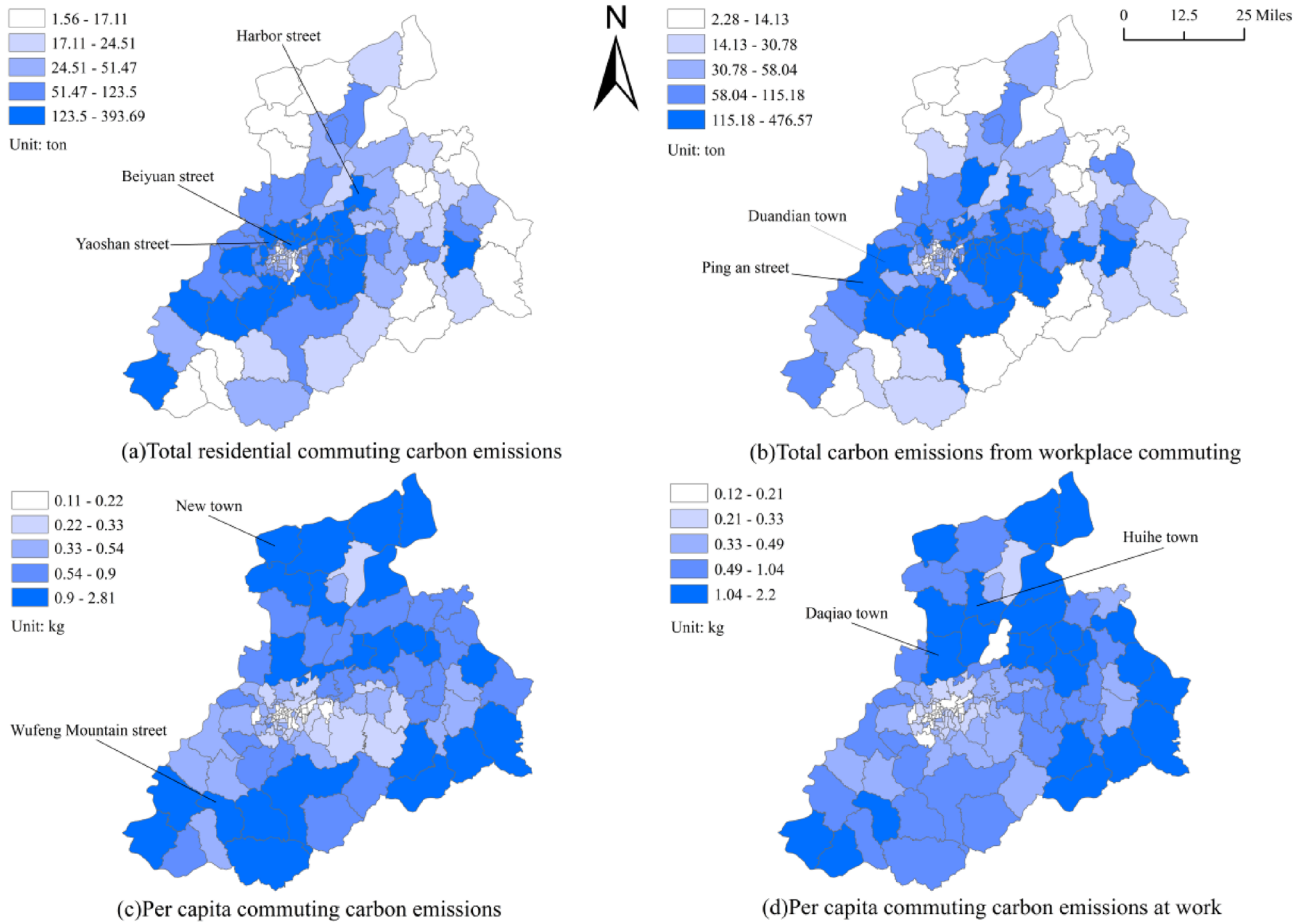


**Fig. 11.** Carbon emission distribution.

*Spatial distribution characteristics of commuting carbon emissions*

Based on the total carbon emissions of residential streets (Fig. 11a), residential streets in the main urban area of Jinan City exhibit unbalanced spatial distribution of carbon emissions. The densely populated areas near the three-ring road, such as Beiyuan Street, Yaoshan Street and Licheng Economic Development Zone, have higher carbon emissions. The residential and commuting carbon emissions of central urban areas and peripheral streets are relatively low. Streets dominated by employment activities have higher carbon emissions (Fig. 11b), with typical examples including Duandian Town, Ping An Street, and Jibei Economic Development Zone. In contrast,

streets with low carbon emissions are primarily concentrated in central districts and peripheral areas with lower employment intensity.

The per capita carbon emission of residential areas show a pattern of lower levels in central urban areas and higher levels in peripheral areas (Fig. 11c). Streets with relatively high per—capita carbon emissions are mainly located in Wufengshan Street in Changqing District, Zhangqiu Economic Development Zone, and new towns in Jiyang County, all of which are part of new town clusters. Areas with relatively high per—capita carbon emissions are concentrated in the northern sector of the city (Fig. 11d), such as Daqiao Town, Huihe Town in Tianqiao District and Shanghe Economic Development Zone, which mainly focus on the processing industry.

#### *Spatial autocorrelation analysis of commuting carbon emissions*

Spatial autocorrelation analysis acts as a bridge between the description of phenomena and the explanation of underlying mechanisms, enhancing the understanding of the spatial distribution of commuting carbon emissions. The clustering map of residential commuting carbon emissions reveals that the inner ring areas of the central zone form a “low-low” (LL) cluster, while streets adjacent to the core area form a “high-low” (HL) cluster. Areas such as Wang She Ren-Tang Ye Street exhibit a “high-high” (HH) clustering pattern (Fig. 12a,b). The central urban area is characterized by relatively short commuting distances and higher public transportation usage. High-value clustering areas are residential areas located closer to the city center, with higher population density and a higher number of long-distance commuters.

In the clustering map of workplace commuting carbon emissions, a large “low-low” (LL) cluster is observed within the third ring road of the central urban area, while the “high-high” (HH) clusters are predominantly concentrated in the eastern and northern new town areas (Fig. 12c,d). In Jinan’s central urban area, a significant proportion of commuters live near their workplaces, a better work-residence balance, and as a result, the total carbon emissions from workplaces are relatively low. Streets such as Shunhua Road and Tangye Street, dominated by high-tech industries, attract a large number of workers and have a considerable impact on surrounding areas, such as Gangou Street and Caishi Town, leading to a high density of long-distance commuters. Consequently, these areas exhibit high workplace commuting carbon emissions.

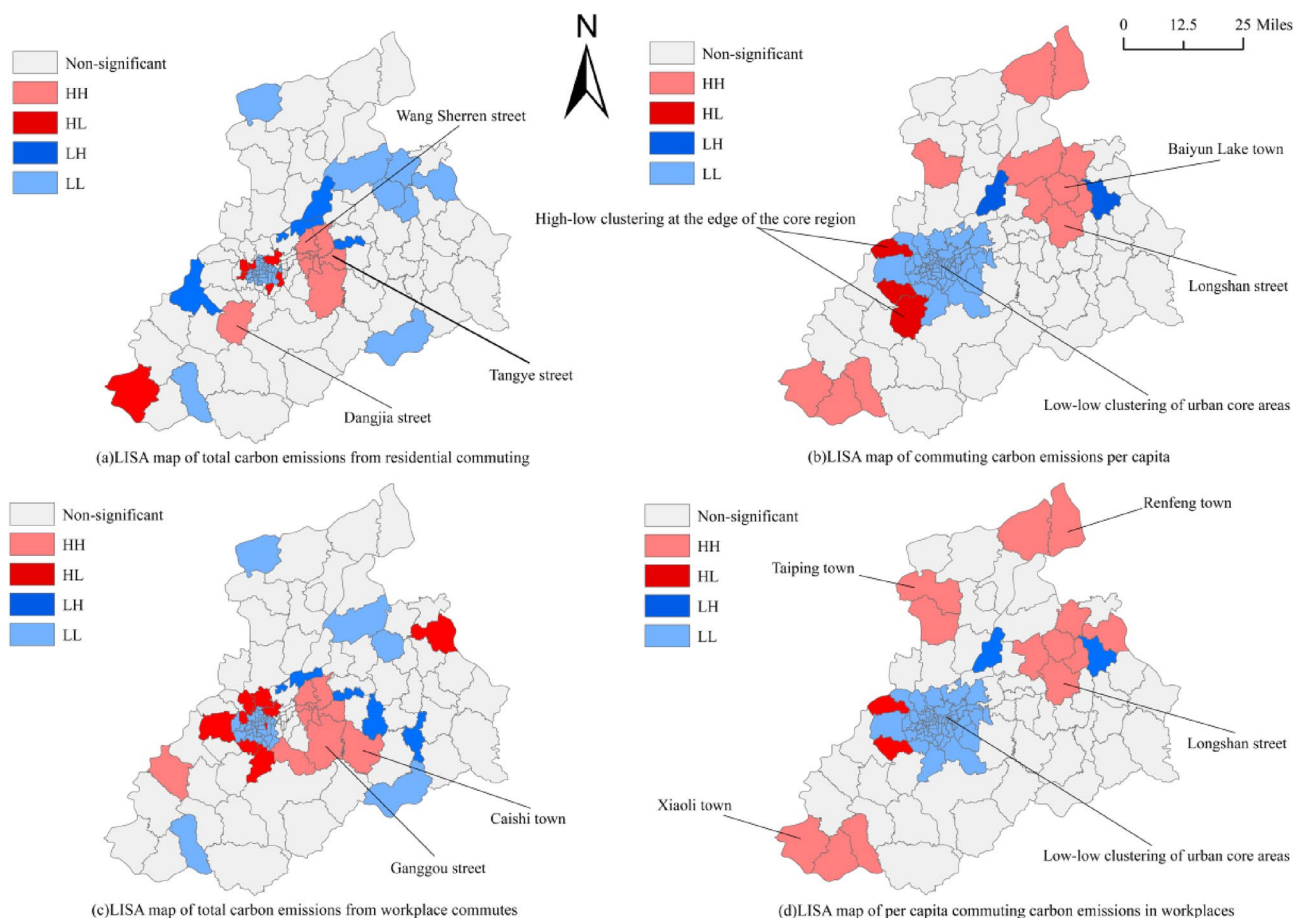


**Fig. 12.** Spatial autocorrelation analysis of commuting carbon emissions.

Independent variable	Linear regression result parameters				
	B	Beta	T	Sig	VIF
Intercept	-1.01	-	-7.22	***	-
Road network density	0.31	0.29	3.01	***	3.45
Number of subway stations	0.28	0.22	2.33	***	3.23
Transportation facilities land proportion	0.24	0.17	1.65	***	2.12
Number of commercial housing	0.41	0.35	2.74	***	4.65
Industrial land proportion	-0.15	-0.11	-1.18	**	1.04
Number of tourist attractions	-0.19	-0.15	-1.31	***	1.13

**Table 6.** Gradual linear regression of total carbon emissions from residential areas.

Independent variable	Linear regression result parameters				
	B	Beta	T	Sig	VIF
Intercept	0.73	-	8.52	***	-
Accessibility	0.25	0.21	2.43	***	2.92
Road network density	-0.22	-0.19	-2.14	***	2.31
Number of commercial housing	-0.16	-0.11	-1.62	***	1.62
Greenness	-0.26	-0.23	-2.12	**	2.71
Safety	-0.13	-0.06	-1.32	**	1.41

**Table 7.** Gradual linear regression of carbon emissions per inhabitant.

## Stepwise linear regression analysis of commuting carbon emissions

### *Gradual linear regression of residential carbon emissions*

According to the coefficients from the stepwise regression analysis (Table 6), the regression coefficients for road network density, the number of subway stations, the proportion of land used for transportation facilities, and the number of commercial and residential units are all positive. This suggests that an increase in road network density, the proportion of land allocated to transportation facilities, the number of subway stations, and the number of commercial and residential units to an increase in residential carbon emissions. The coefficients for industrial land use and tourist attractions are negative. Areas with a higher proportion of industrial land typically exhibit a concentration of employment, leading to shorter work-residence distances. Tourist demand often stimulates the development of public transportation or non-motorized transport systems, thereby reducing carbon emissions.

The regression results indicate that certain perceived elements extracted from streetscapes significantly influence per capita commuting carbon emissions (Table 7). Greenness and Safety demonstrate a significant negative effect on per capita commuting carbon emissions at residential locations. Residential areas with higher greenness generally offer better walking and cycling environments, as well as improved accessibility to public transportation, thereby encourages residents to choose low-carbon travel modes. Streets with higher safety are often equipped with adequate lighting systems, surveillance facilities, and well-designed vehicle-pedestrian separation, all of which promote the use of non-motorized transportation modes.

### *Gradual linear regression of workplace carbon emissions*

According to the partial regression coefficient Beta in the model results (Table 8), the regression coefficients of the number of companies, the length of the road network, the average price of housing, the area of residential land, the number of subway stations and the area of public service facilities are all positive. This indicates that larger areas of residential, commercial, and industrial land and a greater number of transportation stations are associated with higher total workplace carbon emissions.

Based on the standardized coefficients from the regression results, the factors influencing per capita workplace carbon emissions are ranked as follows: Floor Area Ratio > Accessibility > Road Network Density > Number of Tourist Attractions > Openness > Depression (Table 9). Among these, the Floor Area Ratio has the greatest impact, with a more pronounced effect than Accessibility and Road Network Density, while the influence of Depression is the weakest.

## Geographical weighted regression analysis of commuting carbon emissions

### *Geographical weighted regression of residential carbon emissions*

The regression coefficients for the area of land used for transportation facilities and tourist attractions exhibited a gradient increase from the southern to the northern region, with the southern part of the main urban area was mainly negative, while the northern part was mainly positive. The regression coefficients of Longdong-Ganggou and Lingang Economic Development Zone are the largest, indicating that transportation facilities significantly

Independent variable	Linear regression result parameters				
	B	Beta	T	Sig	VIF
Intercept	-1.21	-	-8.42	***	-
Road network density	0.15	0.13	1.3	***	1.47
Number of companies	0.46	0.41	4.24	***	4.32
Average house price	0.27	0.24	2.31	**	2.41
Residential area	0.16	0.13	1.21	***	1.29
Number of shopping consumption	-0.21	-0.18	-2.35	***	2.26
Medical care	0.42	0.36	4.01	**	4.3
Number of subway stations	0.17	0.14	1.29	***	1.67
Public service facilities area	0.13	0.09	1.09	**	1.01

**Table 8.** Gradual linear regression of total workplace carbon emissions.

Independent variable	Linear regression result parameters				
	B	Beta	T	Sig	VIF
Intercept	0.29	-	3.4	***	-
Accessibility	0.31	0.29	3.24	**	3.8
Road network density	-0.26	-0.23	-2.5	***	2.65
Plot ratio	-0.37	-0.31	-3.9	**	3.17
Openness	-0.23	-0.17	-2.06	***	2.56
Number of tourist attractions	-0.22	-0.18	-2.12	***	2.01
Depressing	0.29	0.25	-2.18	**	2.65

**Table 9.** Gradual linear regression of carbon emissions per capita at work site.

source not found.(a).

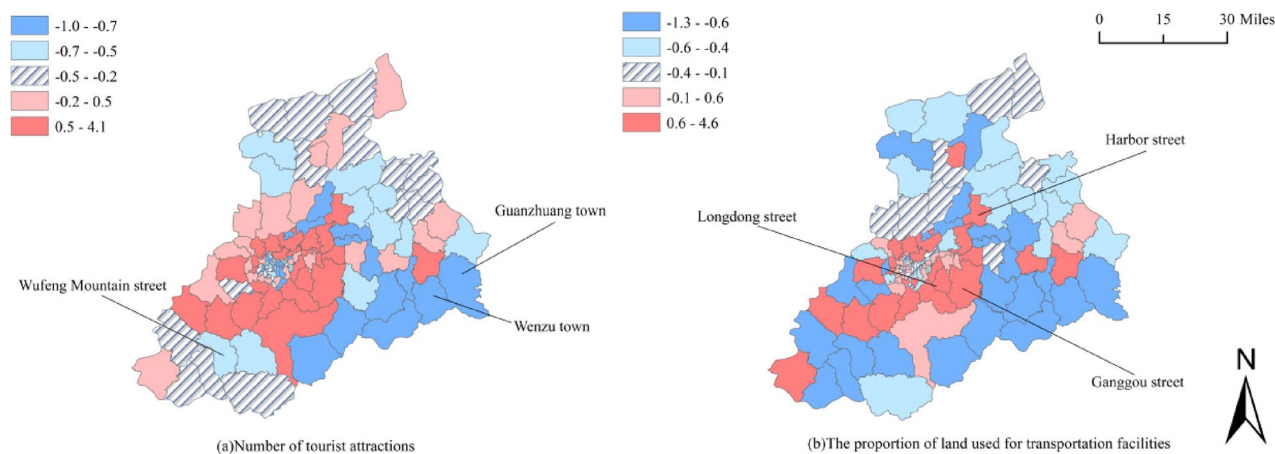


**Fig. 13.** Regression coefficient of GWR model of total carbon emissions from residential areas.

promote residential population agglomeration in these areas (Fig. 13b). Phuket—Guanzhuang, Wenzu town and other areas are close to Zhangqiu Economic Development Zone, have tourism resource endowments comparable to. Residents are more likely to choose to visit nearby, so the regression coefficient is relatively low or negative (Fig. 13a).

For residential areas, Cao Fan Town is situated in an urban–rural fringe area with poor security and inadequate lighting conditions. In industrial areas such as Sun Geng Street, high pollution risks and low perceived safety lead to increased private car use. In contrast, newly developed communities in areas like Zhi Yuan-Yaojia Street, with well-planned infrastructure, have lower safety risks, making residents more inclined to choose non-motorized or green transportation modes (Fig. 14a). Additionally, the regression coefficient for Greenness reveals three distinct distribution patterns: the core urban area (high Greenness + low carbon

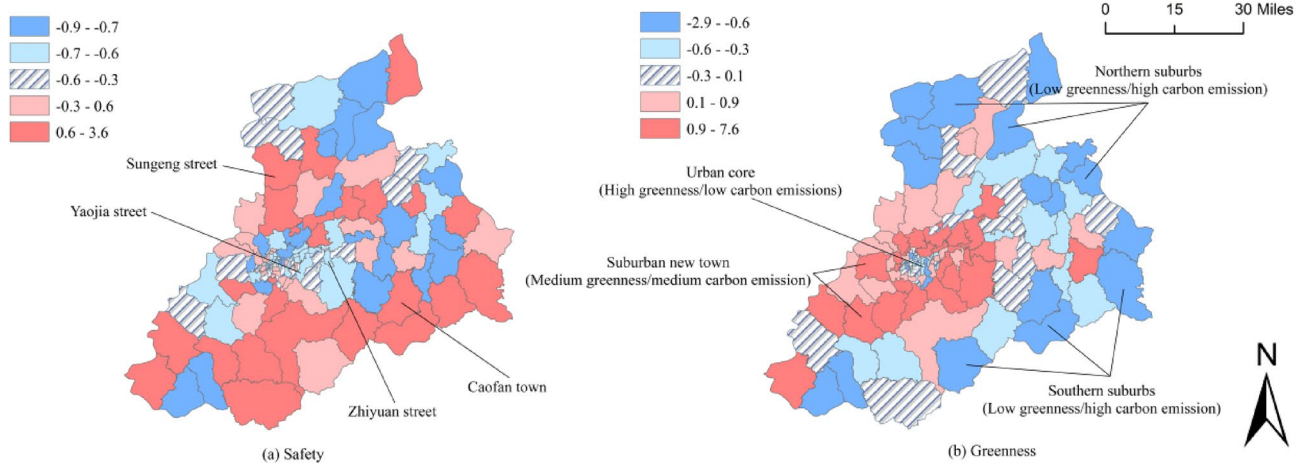


**Fig. 14.** Regression coefficient of GWR model of carbon emissions per inhabitant.

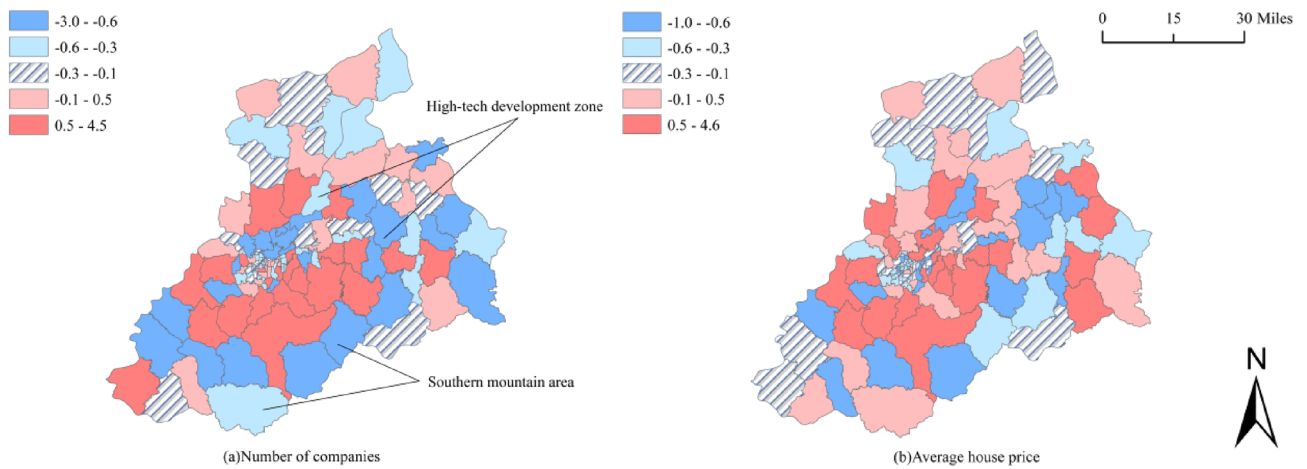


**Fig. 15.** Regression coefficient of GWR model of total carbon emissions from work site.

emissions), the suburban area (medium Greenness + medium carbon emissions), and the outer suburbs (low Greenness + high carbon emissions) (Fig. 14b). In the core urban area, carbon emission reduction is achieved through “short-distance commuting + non-motorized transport dominance”, which drives the detailed layout of green spaces. In suburban new towns, the function of green spaces is mixed and insufficient, requiring reliance on subways and buses for emission reduction. In the outer suburbs, fragmented green spaces lead to higher dependence on private cars.

*Geographical weighted regression of workplace carbon emissions*

The regression coefficient of the southern mountainous area and the eastern new town group is lower than that of other regions (Fig. 15). Tourism is the main industries to be developed in the southern mountain area, high-tech development zones are located in the eastern part of the city, and the new and old energy conversion Zone in the north is China’s second state-level new area after Xiongan New Area, aiming to promote ecological protection and high-quality development of the Yellow River Basin<sup>49</sup>. By appropriately enriching the types of companies and developing low-carbon and environmental protection industries according to local conditions, the total carbon emissions of the workplace can be reduced.

For workplaces, Yaojia Street, Shunyu Road, and Wang She Ren Street are characterized by high-density communities with moderate to low openness. These streets, however, exhibit strong functional diversity, with short-distance commuting being the predominant mode. In contrast, Daqiao Town and Xiying Town, through the development of new ecological areas, maintain a high level of openness. However, these regions are located in the outer suburbs of the city, and long-distance commuting increases carbon emissions (Fig. 16a). Meanwhile, CuiZhai Town, Lingang Street, and other monofunctional singular “dormitory towns”, while creating a sense of residential oppression for residents, also promote the use of private cars (Fig. 16b).

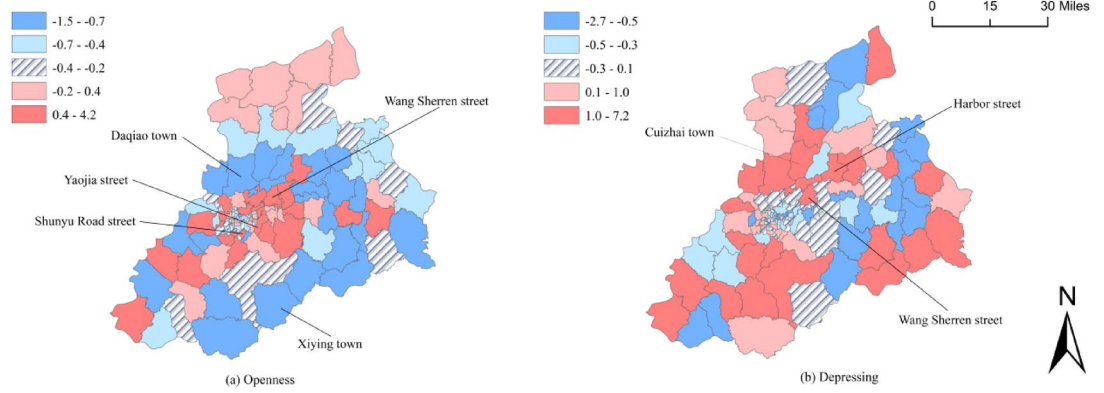


**Fig. 16.** GWR model regression coefficient of per capita carbon emissions at work site.

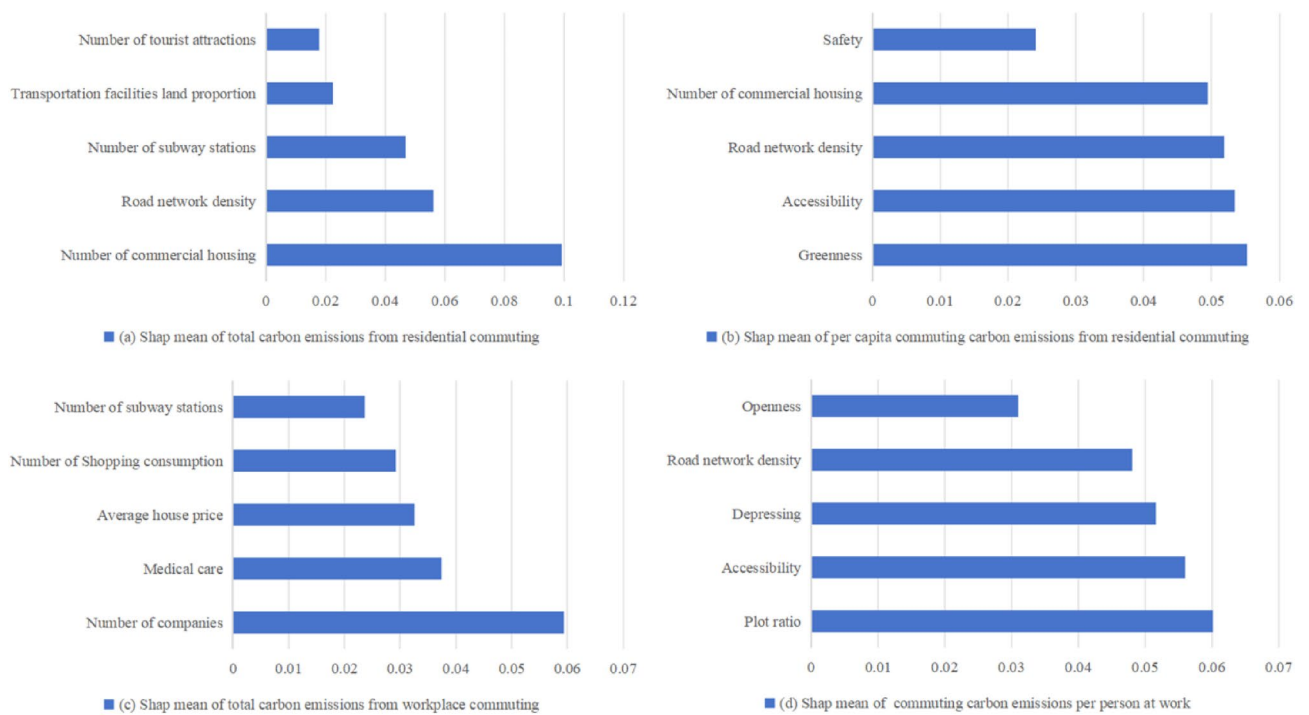


**Fig. 17.** Ranking of Importance Based on XGBoost.

*Importance analysis using XGBoost*

To clarify the effects of the built environment, the XGBoost machine learning method was used to rank the importance of significant independent variables across four models for a comprehensive analysis (Fig. 17). The number of commercial and residential units plays a dominant role in the scale of carbon emissions, with its spatial clustering significantly increasing the separation between work and residence<sup>58</sup>. High-density development reduces pedestrian spaces, leading to greater dependence on private cars<sup>59</sup>. Green vision rate regulates travel patterns through psychological perception<sup>60</sup>, and its mechanism of action forms a synergistic effect with security perception<sup>61</sup> and road network density. The dominance of the number of companies and enterprises stems from the continuous and rigid commuting demand<sup>62</sup>, while the service radius of commercial and medical POIs has localized characteristics<sup>63</sup>. Floor area ratio affects individual choices through dual pathways. Although a high floor area ratio enhances the balance between work and residence<sup>64</sup>, the sense of oppression leads to an increase in motor vehicle preference<sup>65</sup>.

*Two-factor interaction analysis*

In this study, the independent variables selected by multiple linear regression were analyzed by using geographic detector, and bivariate interaction analysis was conducted on total commuting carbon emissions and per capita commuting carbon emissions respectively. Total commuting carbon emissions are primarily influenced by the interaction between the number of commercial and residential units and the proportion of land allocated to

transportation infrastructure (Fig. 18a). Commercial residential land provides housing for individuals engaged in commercial activities, while transportation infrastructure land offers the essential support for these activities<sup>66</sup>. Among the interactive variables affecting per capita commuting carbon emissions, road network density plays the most prominent role (Fig. 18b). High road network density facilitates more convenient transfers between attractions, reducing travel time and enhancing tourism efficiency<sup>67</sup>. Additionally, increased road network density improves access to a broader range of tourist destinations, allowing visitors to experience more diverse attractions<sup>68</sup>.

### Discussion

#### The hierarchical structure of the number of commuters and commuting distance

The commuting population and commuting distances in the central urban area of Jinan exhibit distinct spatial patterns. The commuting distances in both the central urban area and the suburbs are relatively short, and these regions are designated as the “commuting cold zone” in this study. Areas with larger commuting populations and longer commuting distances are primarily concentrated between the second and third rings of the central urban area (Fig. 19a), which are referred to as the “commuting hot zone”. As land resources in the central urban area become increasingly scarce, residential areas have gradually expanded toward the city’s suburbs<sup>69</sup>. This outward expansion has increased the proportion of residential land within the “commuting hot zone”, thereby raising commuting demand. The residential hotspots areas are primarily inhabited by middle- and low-income groups, who frequently commute across regions to employment centers in the city center, while another group commutes to factories or farmlands in the suburbs, requiring longer commuting distances (Fig. 19b). The commuting cold zones in the suburbs are characterized by short commuting times, reflecting the presence of specialized industries such as agriculture, forestry, animal husbandry, and fishery activities, which are spatially dispersed across the suburbs<sup>70</sup> (Fig. 19c). Industries requiring substantial labor and capital investment, such as manufacturing and construction, are typically concentrated in specific industrial parks.

#### Differences in the spatial impact of street perception characteristics on total and per capita commuting carbon emissions

The results of spatial analysis indicate that the influence of street perception characteristics on per capita commuting carbon emissions is significantly stronger than their impact on total commuting carbon emissions. Per capita carbon emissions reflect individuals’ commuting behavior patterns and are directly influenced by their travel choices<sup>71</sup>. Street perception characteristics can significantly influence individuals’ travel modes by shaping residents’ subjective experiences and decisions, thereby reducing per capita carbon emissions. Total carbon emissions are comprehensively influenced by the size of the regional population, the scale of economic activities, and commuting demands<sup>72</sup>. Even if per capita emissions decline, when the population grows or commuting demand increases, total emissions may rise rather than fall. The influence of street perception characteristics on total emissions is indirectly reflected through “individual behavior change × population size”, and its effect is easily diluted by macro trends.

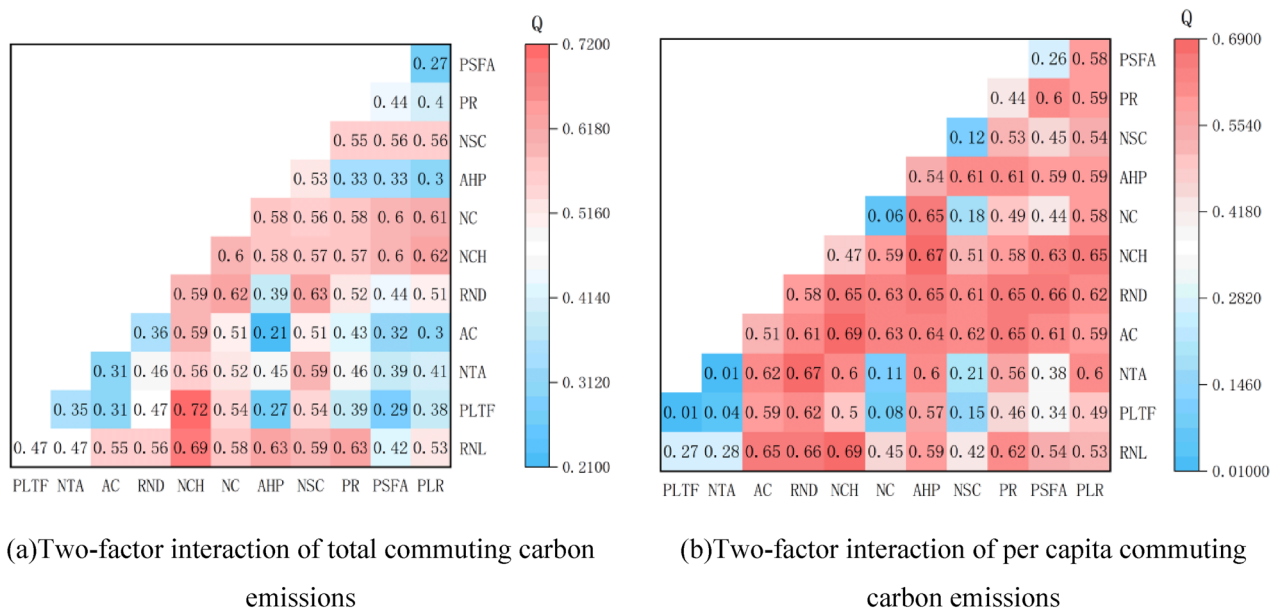


**Fig. 18.** Interaction analysis of commuting carbon emissions. The picture is self-drawn by the author.

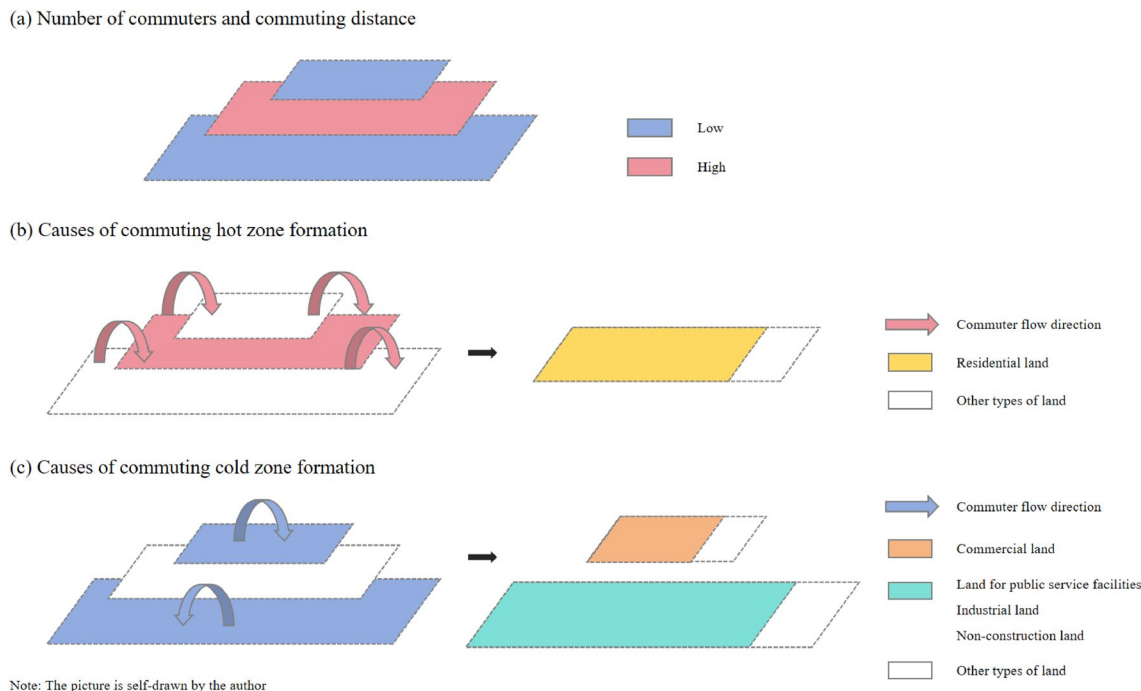


**Fig. 19.** Commuter cold zone and commuter hot zone.

### Emission reduction efficiency of tourist attractions in the core area and the low-carbon renewal model

We observed that the negative impact of tourist attractions on carbon emissions in Jinan's core area is greater than that of transportation facilities. Tourist attractions in the core area serve not only as visiting nodes but also restructure urban functions through a mixed development model of "business, tourism, culture, and residence"<sup>73</sup>. Scenic spots have created a large number of service industry jobs (such as tour guides, catering, and retail), among which the night economy has further promoted the adoption of flexible working systems, increased the proportion of off-peak commuting, and reduced idle carbon emissions caused by peak-hour congestion<sup>73</sup>. The practice in Jinan's core area demonstrates that in high-density built-up areas, catalytic mixed-use development of scenic spots achieves far greater emission reduction efficiency than upgrading traditional transportation facilities. This provides a low-carbon renewal model for similar historical cities (e.g., Xi'an and Luoyang): rather than infinitely expanding transportation supply, it is better to activate the intrinsic carbon reduction potential of existing resources through "spatial acupuncture".

### The differentiated impact of openness and spatial depression on suburban street commuting carbon emissions

The opposing effects of Openness and Spatial Depression on commuting carbon emissions in suburban areas stem from the complex interaction between urban form, behavioral psychology, and transportation patterns. Wide streets with continuous green belts can reduce psychological resistance to walking or cycling, increasing the share of slow commuting<sup>74</sup>. In contrast, depressed streets (characterized by confined spaces) often coincide with inefficient road networks, posing detour risks during commuting. Frequent roadside parking further encroaches on slow-moving spaces. Such confined environments often trigger elevated cortisol levels, making residents more inclined to drive to avoid environmental stress. For future suburban urban renewal, environmental psychology indicators (e.g., sky visibility and green view index) should be integrated into the statutory planning system. Integrating digital twin technology to simulate the emission reduction effects of visual interventions can achieve coordinated progress in "spatial healing" and "carbon emission reduction".

### Conclusion

This study focuses on the central urban area of Jinan, with the primary aim of analyzing the relationship between commuting carbon emissions and the built environment. It utilizes multiple data sources, including commuting trajectories and street view images, to collect data on commuting carbon emissions and the built environment. Using a methodological framework that includes linear selection, spatial autocorrelation and geographically weighted regression, XGBoost importance ranking, and geographic detector interaction analysis, this research investigates the impact of the built environment on commuting carbon emissions. The goal is to provide theoretical insights for urban planning and development in medium-sized cities. The research findings are as follows:

- (1) Based on the current situation of commuter connections, the per capita commuting distance in the main urban area of Jinan City is 6 km, and private vehicles are the main commuting mode. The proportion of commuting by bus, bike and car is 22%, 38% and 40% respectively. The spatial distribution of the driving proportion and per capita commuting distance exhibits the characteristics of “low in the center and high in the periphery”.
- (2) From the perspective of spatial characteristics, streets with higher total carbon emissions in residential areas are primarily concentrated in the residential clusters near the Third Ring Road. Meanwhile, streets with high total carbon emissions in the workplace are mostly employment oriented streets such as Yanshan Street, Jiyang Street, and Yanwen Community. In residential areas, streets with higher per capita carbon emissions are located in the Changling Mountain area, Shengfu Zhuang area, and Lianhua Mountain area. The low-value cluster area is primarily situated within the central urban zone, whereas the high-value cluster area displays a markedly different distribution pattern.
- (3) The regression results reveal significant spatial heterogeneity in the driving factors of commuting carbon emissions, with the impact of transportation infrastructure land on total carbon emissions exhibiting a north–south gradient. In residential areas, perceived safety and greenness levels show a spatial coupling effect. The greenness coefficient exhibits hierarchical differentiation among the central urban area, the near suburbs, and the far suburbs. Workplace carbon emissions are primarily influenced by the spatial functional composition, with high-density mixed-use communities achieving low-carbon emissions through short-distance commuting. The openness coefficient exhibits contrasts in areas characterized by a single function. Carbon emission intensity in the southern mountainous, tourist-oriented areas is lower than in the industrially dominated eastern new town, confirming the regulatory effect of industrial type on the carbon emission baseline.
- (4) Regarding the order of importance of factors and their interactive effects, the number of commercial and residential units and enterprise agglomeration are the dominant factors for total carbon emissions at residential and workplace locations, respectively. Per capita emissions are more influenced by individual behavior and environmental interactions. Furthermore, commercial and residential areas and transportation infrastructure land exhibit a complementary effect, while the strong interaction between road network density and tourist attractions highlights the capacity of high-density road networks to enhance tourism efficiency.

The study suggests that policymakers should implement differentiated spatial governance based on the north–south (east–west) gradient effects of the city, promoting “TOD + work-residence balance” development. Green space optimization should be prioritized, with the core urban area advancing the “500-m green view” project and the far suburbs developing ecological corridors to reduce green space fragmentation. A “carbon emission—spatial perception” monitoring platform should be established, integrating mobile signaling and street view data to track latent perceptual factors in real time.

There are some limitations to the data in this study. On the one hand, the study calculated the carbon emission index based on big data of commuting trajectory, but commuting modes were only divided into driving, public transportation and cycling, which were not detailed enough compared with the questionnaire survey. On the other hand, using streets as the research unit, this study may encounter the modifiable areal unit problem (MAUP), which can have uncertain effects on the results of spatial data analysis and thus affect the accuracy of the correlation analysis between built environment factors and commuting carbon emissions to a certain extent. Therefore, the next step involves establishing a grid using geographic information technology to more accurately measure the built environment of residential and workplace locations. A multi-scale analysis framework, such as “city-district-street-living circle-grid”, can be constructed, with appropriate geographical units selected to define scales and partitions, thereby enriching the conclusions and enhancing the accuracy of the research.

## Data availability

All data generated or analysed during this study are included in its supplementary information files.

Received: 27 February 2025; Accepted: 12 May 2025

Published online: 15 May 2025

## References

1. Song, Y. et al. Strategies and pathways of the transport sector for addressing climate change. *Journal of Tsinghua University (Natural Science Edition)* **63**(11), 1501–1510. <https://doi.org/10.16511/j.cnki.qhdxxb.2023.26.021> (2023).
2. Xu, W., Hua, G., & Huang, A. Analysis on carbon emission reduction potential of China's highway transportation under the background of vehicle electrification. In *International Conference on Logistics, Informatics and Service Sciences* 639–653. (Springer, 2023).
3. Xiong, S., Yuan, Y. & Zhang, C. Achievement of carbon peak goals in China's road transport—possibilities and pathways. *J. Clean. Prod.* **388**, 135894 (2023).
4. Lu, Q. et al. Decarbonization scenarios and carbon reduction potential for China's road transportation by 2060. *npj Urban Sustain.* **2**(1), 34 (2022).
5. Gao, C., Lai, X., Li, S., Cui, Z. & Long, Z. Bibliometric insights into the implications of urban built environment on travel behavior. *ISPRS Int. J. Geo Inf.* **12**(11), 453 (2023).
6. Gim, T. H. T. Analyzing the city-level effects of land use on travel time and CO<sub>2</sub> emissions: A global mediation study of travel time. *Int. J. Sustain. Transp.* **16**(6), 496–513 (2022).
7. Yang, Y. Research on the impact of built environment on commuting carbon emissions based on spatiotemporal big data (Master's Thesis, Wuhan University). <https://doi.org/10.27379/d.cnki.gwhdu.2022.000642>. (2022).
8. Lu, M. & Diab, E. Understanding the determinants of x-minute city policies: a review of the North American and Australian cities' planning documents. *J. Urban Mobil.* **3**, 2667–0917 (2022).

9. Khavarian-Garmsir, A. R., Sharifi, A. & Sadeghi, A. The 15-minute city: Urban planning and design efforts toward creating sustainable neighborhoods. *Cities* **132**, 104101 (2023).
10. Uddin, M. A. et al. A framework to measure transit-oriented development around transit nodes: Case study of a mass rapid transit system in Dhaka, Bangladesh. *PLoS ONE* **18**(1), e0280275 (2023).
11. Chen, J., Tian, W., Xu, K. & Pellegrini, P. Testing small-scale vitality measurement based on 5D model assessment with multi-source data: A resettlement community case in Suzhou. *ISPRS Int. J. Geo Inf.* **11**(12), 626 (2022).
12. Zhang, Q. W. (2024). Research on the influencing factors of residents' commuting carbon emissions and optimization strategies under the slow mobility orientation of residential areas (Master's Thesis, North China University of Technology). <https://doi.org/10.26926/d.cnki.gbfgu.2024.000102>. (2024).
13. Liu, J. et al. Multi-scale urban passenger transportation CO2 emission calculation platform for smart mobility management. *Appl. Energy* **331**, 120407 (2023).
14. Kissinger, M. & Reznik, A. Detailed urban analysis of commute-related GHG emissions to guide urban mitigation measures. *Environ. Impact Assess. Rev.* **76**, 26–35 (2019).
15. Dong, Q. et al. How building and street morphology affect CO2 emissions: Evidence from a spatially varying relationship analysis in Beijing. *Build. Environ.* **236**, 110258 (2023).
16. Pan, B. et al. The relationship between three-dimensional spatial structure and CO2 emission of urban agglomerations based on CNN-RF modeling: A case study in East China. *Sustainability* **16**(17), 7623 (2024).
17. Chen, B. et al. Mapping essential urban land use categories with open big data: Results for five metropolitan areas in the United States of America. *ISPRS J. Photogramm. Remote Sens.* **178**, 203–218 (2021).
18. Zhao, Z. & Liang, Y. A deep inverse reinforcement learning approach to route choice modeling with context-dependent rewards. *Transp. Res. Part C Emerg. Technol.* **149**, 104079 (2023).
19. Sun, H. et al. A Spatial analysis of urban streets under deep learning based on street view imagery: quantifying perceptual and elemental perceptual relationships. *Sustainability* **15**(20), 14798 (2023).
20. Bin, J., Gardiner, B., Li, E. & Liu, Z. Multi-source urban data fusion for property value assessment: A case study in Philadelphia. *Neurocomputing* **404**, 70–83 (2020).
21. Ma, Y., Zhao, S., Wang, W., Li, Y. & King, I. Multimodality in meta-learning: A comprehensive survey. *Knowl. Based Syst.* **250**, 108976 (2022).
22. Qi-xiang, C. H. E. N., Bin, L. Y. U. & Xian-lin, L. I. Nonlinear effect of station-area built environment on taxi-metro combined travel. *J. Traff. Transp. Eng.* **24**(5), 285–300. <https://doi.org/10.19818/j.cnki.1671-1637.2024.05.019> (2024).
23. Zhang, L., Wang, K. & Yu, J. L. Optimization of job-housing spatial distribution for non-registered populations in megacity metropolitan areas: A case study of Beijing and Chengdu, China. *Ancient City* **39**(1), 3–8. <https://doi.org/10.19924/j.cnki.1674-4144.2025.001.001> (2025).
24. Huai, Y., Lo, H. K. & Ng, K. F. Monocentric versus polycentric urban structure: Case study in Hong Kong. *Transp. Res. Part A Policy Pract.* **151**, 99–118 (2021).
25. Eom, H. Does job accessibility matter in the suburbs? Black suburbia, job accessibility, and employment outcomes. *Land* **11**(11), 1952 (2022).
26. Dong, K., Jia, R., Zhao, C. & Wang, K. Can smart transportation inhibit carbon lock-in? The case of China. *Transp. Policy* **142**, 59–69 (2023).
27. Karakadzai, T., Bandaiko, E., Chaeruka, J. & Arku, G. Examining the conformance of development to local spatial plans amid rapid urbanisation in Harare, Zimbabwe. *Land Use Policy* **126**, 106543 (2023).
28. Peng, W. B. & Cao, X. T. Temporal and spatial differentiation of ecological resilience and its influence effects under the role of urban renewal: A case study of the Changsha-Zhuzhou-Xiangtan urban agglomeration. *Econ. Geogr.* **43**(10), 44–52. <https://doi.org/10.15957/j.cnki.jjdl.2023.10.005> (2023).
29. Lu, Q., Ning, J., You, H. & Xu, L. Urban intensity in theory and practice: Empirical determining mechanism of floor area ratio and its deviation from the classic location theories in Beijing. *Land* **12**(2), 423. <https://doi.org/10.3390/land12020423> (2023).
30. Zhao, C., Dong, K., Zheng, S., Fu, X. & Wang, K. Can China's aviation network development alleviate carbon lock-in?. *Transp. Res. Part D Transp. Environ.* **115**, 103578 (2023).
31. Zhang, J. et al. Spatial accessibility and equality of public medical facilities in rural areas based on the improved 3SFCA: A case of Haikou City. *Prog. Geogr.* **41**(4), 636–647 (2022).
32. Gong, P. et al. Mapping essential urban land use categories in China (EULUC-China): Preliminary results for 2018. *Sci. Bull.* **65**(3), 182–187 (2020).
33. Wan, R. X. et al. Study on the temporal and spatial characteristics and influencing factors of carbon emissions from energy consumption in county areas of Shandong province. *Acta Sci. Circumstant.* **18**(12), 3405–3413 (2024).
34. Liu, B., Chang, H., Li, Y. & Zhao, Y. Analysis of influencing factors of industrial green and low-carbon transformation under the background of “double carbon”: Evidence from Sichuan province, China. *Front. Environ. Sci.* **11**, 1257855 (2023).
35. Liu, J. et al. Matching network advantages and configuration improvement paths for green innovation development in regional tourism: A case study of the Shandong Peninsula urban agglomeration. *Acta Ecol. Sin.* **45**(2), 493–510. <https://doi.org/10.20103/j.stxb.202405121072> (2025).
36. Qingchun, L. I. U., Wenli, Z. O. N. G., Peixiong, Z. H. A. O., Yanan, S. U. N. & Jiaoguo, M. A. Research on the evolution characteristics and influencing factors of urban network structure in Shandong Province based on the connection of listed enterprises. *World Reg. Stud.* **33**(4), 88 (2024).
37. Zhang, M. & Zhou, Y. Analysis of the characteristics of the spatial association network of carbon emission efficiency of urban construction land and its influencing factors: A case study of Shandong Province. *Resour. Dev. Market* **39**(11), 1449–1457 (2023).
38. Fan, W. P., Zhang, J., Wang, J. H. & Shan, B. Y. The pattern and optimization of the transportation network of the three major economic circles in Shandong province from the perspective of syntax. *Geogr. Geo Inf. Sci.* **39**(01), 55–61 (2023).
39. Brand, C. & Preston, J. M. '60-20 emission'—The unequal distribution of greenhouse gas emissions from personal, non-business travel in the UK. *Transp. Policy* **17**(1), 9–19 (2010).
40. He, K., Zhang, X., Ren, S., & Sun, J. Deep residual learning for image recognition. In *Proceedings of the IEEE Conference on Computer Vision and Pattern Recognition*. 770–778. (2016).
41. Chen, L. C., Papandreou, G., Kokkinos, I., Murphy, K. & Yuille, A. L. Deeplab: Semantic image segmentation with deep convolutional nets, atrous convolution, and fully connected crfs. *IEEE Trans. Pattern Anal. Mach. Intell.* **40**(4), 834–848 (2017).
42. Chen, L. C., Zhu, Y., Papandreou, G., Schroff, F., & Adam, H. Encoder-decoder with atrous separable convolution for semantic image segmentation. In *Proceedings of the European Conference on Computer Vision (ECCV)*. 801–818. (2018).
43. Ma, X. et al. Measuring human perceptions of streetscapes to better inform urban renewal: A perspective of scene semantic parsing. *Cities* **110**, 103086 (2021).
44. Dai, L. et al. Analyzing the correlation between visual space and residents' psychology in Wuhan, China using street-view images and deep-learning technique. *City Environ. Interact.* **11**, 100069 (2021).
45. Wang, L., Han, X., He, J. & Jung, T. Measuring residents' perceptions of city streets to inform better street planning through deep learning and space syntax. *ISPRS J. Photogramm. Remote Sens.* **190**, 215–230 (2022).
46. Yao, Y. et al. A human-machine adversarial scoring framework for urban perception assessment using street-view images. *Int. J. Geogr. Inf. Sci.* **33**(12), 2363–2384 (2019).

47. Wang, T., Du, F., Ding, K., Qin, W. & Sun, L. Examining the relationship between the built environment and carbon emissions from operating vehicles: enlightenment from nonlinear models. *Environ. Sci. Pollut. Res.* **31**, 1–13 (2024).
48. Ashik, F. R., Rahman, M. H., Antipova, A. & Zafri, N. M. Analyzing the impact of the built environment on commuting-related carbon dioxide emissions. *Int. J. Sustain. Transp.* **17**(3), 258–272 (2023).
49. Zhao, C. et al. Impact of residential land use function mix on residents' travel behavior from the perspective of carbon emissions: A case study of Gaoshui District in Mianyang, China. In *International Conference on Urban Climate, Sustainability and Urban Design* (eds He, Bao-Jie. et al.) 390–401 (Springer, 2023).
50. Liu, Q., Zhao, P., Zhang, Y., Zhang, Z. & Yang, J. Estimating the non-linear effects of urban built environment at residence and workplace on carbon dioxide emissions from commuting. *Front. Public Health* **10**, 1077560 (2022).
51. Lin, J., He, X., Lu, S., Liu, D. & He, P. Investigating the influence of three-dimensional building configuration on urban pluvial flooding using random forest algorithm. *Environ. Res.* **196**, 110438 (2021).
52. Zhang, F., Deng, X., Phillips, F., Fang, C. & Wang, C. Impacts of industrial structure and technical progress on carbon emission intensity: Evidence from 281 cities in China. *Technol. Forecast. Soc. Chang.* **154**, 119949 (2020).
53. Wang, S., Ren, H., Liang, L., Li, J. & Wang, Z. The effect of economic development on carbon intensity of human well-being: Evidence from spatial econometric analyses. *J. Clean. Prod.* **364**, 132632 (2022).
54. Zhao, K., Qi, M., Yan, X., Li, L. & Huang, X. Dynamic impact of urban built environment on land surface temperature considering spatio-temporal heterogeneity: A perspective of local climate zone. *Land* **12**(12), 2148 (2023).
55. Brunson, C., Fotheringham, A. S. & Charlton, M. E. Geographically weighted regression: a method for exploring spatial nonstationarity. *Geogr. Anal.* **28**(4), 281–298 (1996).
56. Gao, Z. et al. Characteristics of spatial correlation network structure and carbon balance zoning of land use carbon emission in the Tarim River Basin. *Land* **13**(11), 1952 (2024).
57. Lv, Y., Zhu, Z. Y., Guo, X. Y. & Zhu, Z. Y. A user ranking model based on answer quality in online Q&A platforms: A case study of Zhihu. *Acta Stat. Sin.* **42**(05), 761–774. <https://doi.org/10.13860/j.cnki.sltj.20230919-005> (2023).
58. Li, Z. H., Wu, H. W. & Wu, F. Impacts of urban forms and socioeconomic factors on CO<sub>2</sub> emissions: A spatial econometric analysis. *J. Clean. Product.* **372**, 133722 (2022).
59. Oliva, J. & Camarero, L. Accessibility, car dependence and rural peripheralization: The automobility gap in the Spanish countryside. *Sociol. Rural.* **65**(1), e12505 (2025).
60. Xu, J. X., Chen, X. L., Liu, K. L. & Chen, J. Spatial heterogeneous effects of community built environment on the active travel of the elderly. *J. Beijing Jiaotong Univ.* **47**(03), 103–111 (2023).
61. Yao, X. Y., Liu, J., Wang, X. Q., Xiao, Y. & Qi, G. Q. Transition toward driverless robotaxi: Role of social anxiety, perceived safety, and travel habit. *Transp. Res. Part F Psychol. Behav.* **109**, 1402–1418 (2025).
62. Broyer, E. Commuting to the urban tech campus: Tech companies' and their elite workers' co-production of South Lake Union, Seattle. *Urban Stud.* **61**(11), 2118–2134 (2024).
63. Niu, Q., Zhu, F. Z., & Liang, X. Q. Influence exploration of central city industries on the employment spatial distribution of intercity commuting population under the background of metropolitan area integration: A case study of Wuhan Metropolitan Area. *World Regional Studies*, 1–18.
64. Jing, G. S. & Song, C. Exploration of the collaboration between data-driven urban renewal and traffic governance: A case study of Guangzhou City. *Urban Dev. Stud.* **31**(05), 48–55 (2024).
65. Qian, C. Y. Study on the Landscape Evaluation of Shanghai's Living-type Boulevard (Master's Thesis, Shanghai Jiao Tong University). <https://doi.org/10.27307/d.cnki.gsjtu.2016.005005>. (2016).
66. Raimbault, J. An interdisciplinary bibliometric analysis of models for land-use and transport interactions. Preprint at <https://arXiv.org/abs/2102.13501>. (2021).
67. Gao, J., Shao, C. & Chen, S. Evolution and driving factors of the spatiotemporal pattern of tourism efficiency at the provincial level in China based on SBM–DEA model. *Int. J. Environ. Res. Public Health* **19**(16), 10118. <https://doi.org/10.3390/ijerph191610118> (2022).
68. Gao, J. & Wu, B. Revitalizing traditional villages through rural tourism: A case study of Yuanjia Village, Shaanxi Province, China. *Tour. Manage.* **63**, 223–233. <https://doi.org/10.1016/j.tourman.2017.04.003> (2017).
69. Zhang, Y. & Zhao, X. The impact of urban expansion on land use and ecosystem services: A case study of Wuhan, China. *Ecol. Indic.* **125**, 107555. <https://doi.org/10.1016/j.ecolind.2021.107555> (2021).
70. Zhu, W. (2022). Research on the impact of suburbanization on the changes of residential and employment functions in suburbs (Doctoral Dissertation, Capital University of Economics and Business). <https://doi.org/10.27338/d.cnki.gsjmu.2022.000127>
71. Wang, L., Wang, J., Shen, P., Liu, S. & Zhang, S. Low-carbon travel behavior in daily residence and tourism destination: based on TPB-ABC integrated model. *Sustainability* **15**(19), 14349 (2023).
72. Guo, H. Impact of population mobility on regional carbon emissions: empirical evidence from Australia. *Front. Environ. Sci.* **12**, 1392267 (2024).
73. Shao, Y. & Sun, Y. Governing for spatial reconfiguration in tourism-oriented peri-urban villages: New developments from three cases in China. *Buildings* **13**(2), 519 (2023).
74. Schneider, R. J., Wiers, H. & Schmitz, A. Perceived safety and security barriers to walking and bicycling: insights from milwaukee. *Transp. Res. Rec.* **2676**(9), 325–338 (2022).

## Acknowledgements

This study was supported by the National Social Science Fund of China (Grant No.23XMZ045).

## Author contributions

Y. L.: Conceptualization, Methodology, Data curation, Formal analysis, Validation, Visualization, Writing—original draft, Writing—review & editing. Z. L.: Resources, Methodology, Data curation. M. Z.: Methodology, Data curation, Visualization. Y. L.: Resources, Formal analysis, Visualization. J. Y.: Conceptualization, Resources, Methodology, Supervision, Funding acquisition, Writing—review & editing. All authors reviewed the manuscript.

## Declarations

## Competing interests

The authors declare no competing interests.

## Additional information

**Supplementary Information** The online version contains supplementary material available at <https://doi.org/10.1038/s41598-025-02249-8>

[0.1038/s41598-025-02249-8](https://doi.org/10.1038/s41598-025-02249-8).

**Correspondence** and requests for materials should be addressed to J.Y.

**Reprints and permissions information** is available at [www.nature.com/reprints](http://www.nature.com/reprints).

**Publisher's note** Springer Nature remains neutral with regard to jurisdictional claims in published maps and institutional affiliations.

**Open Access** This article is licensed under a Creative Commons Attribution-NonCommercial-NoDerivatives 4.0 International License, which permits any non-commercial use, sharing, distribution and reproduction in any medium or format, as long as you give appropriate credit to the original author(s) and the source, provide a link to the Creative Commons licence, and indicate if you modified the licensed material. You do not have permission under this licence to share adapted material derived from this article or parts of it. The images or other third party material in this article are included in the article's Creative Commons licence, unless indicated otherwise in a credit line to the material. If material is not included in the article's Creative Commons licence and your intended use is not permitted by statutory regulation or exceeds the permitted use, you will need to obtain permission directly from the copyright holder. To view a copy of this licence, visit <http://creativecommons.org/licenses/by-nc-nd/4.0/>.

© The Author(s) 2025